2-deoxyglucose transiently inhibits yeast AMPK signaling and triggers glucose transporter endocytosis, potentiating the drug toxicity

Clotilde Laussel, Véronique Albanèse, Francisco Javier García-Rodríguez, Alberto Ballin, Quentin Defenouillère, Sébastien Léon

2-deoxyglucose inhibits yeast AMPK signaling and triggers glucose transporter endocytosis, potentiating the drug toxicity

Clotilde Laussel[#1], Véronique Albanèse[#1], Francisco Javier García-Rodríguez[1], Alberto Ballin[1], Quentin Defenouillère[1], Sébastien Léon[1,2]

Affiliations:

[#]: Equal contributions
[1]: Université Paris Cité, CNRS, Institut Jacques Monod, F-75013, Paris, France.

[2]: Author for correspondence:

Sébastien Léon, PhD
Institut Jacques Monod
15 Rue Hélène Brion
75205 Paris cedex 13, France.
email: sebastien.leon@ijm.fr ; tel. +33 (0)1 57 27 80 57.

Running title:

Effects of 2-deoxyglucose on yeast AMPK signaling and endocytosis, and contribution to 2DG tolerance

Abstract

2-deoxyglucose is a glucose analog that impacts many aspects of cellular physiology. After its uptake and its phosphorylation into 2-deoxyglucose-6-phosphate (2DG6P), it interferes with several metabolic pathways including glycolysis and protein N-glycosylation. Despite this systemic effect, resistance can arise through strategies that are only partially understood. In yeast, 2DG resistance is often associated with mutations causing increased activity of the yeast 5'-AMP activated protein kinase (AMPK), Snf1. Here we focus on the contribution of a Snf1 substrate in 2DG resistance, namely the alpha-arrestin Rod1 involved in nutrient transporter endocytosis. We report that 2DG triggers the endocytosis of many plasma membrane proteins, mostly in a Rod1-dependent manner. Rod1 is central to 2DG-induced endocytosis because 2DG, following its phosphorylation by hexokinase Hxk2, triggers changes in Rod1 post-translational modifications and promotes its function in endocytosis. Mechanistically, this is explained by a transient, 2DG-induced activation of protein phosphatase 1 (PP1) and a concomitant inactivation of Snf1/AMPK. We show that 2DG-induced endocytosis is detrimental to cells, and the lack of Rod1 counteracts this process by stabilizing glucose transporters at the plasma membrane. This facilitates glucose uptake, which may help override the metabolic blockade caused by 2DG, and 2DG export - thus terminating the process of 2DG detoxification. Altogether, these results shed a new light on the regulation of AMPK signaling in yeast and highlight a remarkable strategy to bypass 2DG toxicity involving glucose transporter regulation.

Introduction

2DG is a glucose analog which lacks a hydroxyl group in position 2, and mainly acts as a competitive inhibitor of glucose metabolism [1]. As such, it competes with glucose for entry into cells and for its subsequent phosphorylation by hexokinase, but is almost not further metabolized. This leads to the intracellular accumulation of 2DG-6-phosphate, a toxic metabolite that inhibits glycolysis and thus leads to a rapid depletion of ATP stores, and the activation of nutrient starvation-activated pathways such as 5'-AMP activated protein kinase, AMPK [2]. Moreover, since mannose is the C2 epimer of glucose, 2-deoxyglucose is also 2-deoxymannose and thus also interferes with mannose metabolism, notably inhibiting protein N-glycosylation [reviewed in 3]. This causes a series of cellular effects, and triggers the onset of the Unfolded Protein Response pathway to face the stress encountered by a defective glycosylation of proteins at the endoplasmic reticulum, which is reportedly the main toxic effect of 2DG in some conditions [4].

The realization that many cancer cells display an aberrantly high glucose uptake and metabolism has led to the idea that glycolysis inhibitors could be used to preferentially target and kill tumor cells [5]. This also allowed the use of radiolabeled glucose derivatives, such as 18-fluoro-2-deoxyglucose, to preferentially label tumors for cancer imaging (PET-scans) [6]. So far, trials using 2DG as the sole chemotherapeutic agent have failed because of the relative toxicity of this molecule, however strategies using 2DG or other 2-deoxy-substituted versions of glucose in combination with other drugs are under study and are promising [6].

2DG has also been extensively used to understand glucose signaling in micro-organisms such as the baker's yeast *Saccharomyces cerevisiae*, where it has been instrumental to delineate the molecular mechanisms by which glucose regulates gene expression [reviewed in 3]. The metabolism of *S. cerevisiae* is biased towards the preferential use of glucose as a carbon source. At the molecular level, glucose represses the expression of many genes involved in respiratory metabolism or in the use of other carbon sources, thereby favoring the preferential use of glucose by fermentation [7]. Among the actors in charge of adapting the transcriptional program with respect to glucose availability is the yeast orthologue of AMPK, Snf1 [7, 8]. Snf1 is the catalytic subunit of a heterotrimeric complex which is active in the absence of glucose in the medium. A canonical example of a Snf1-regulated transcription is that of the invertase *SUC2*, required for sucrose hydrolysis and metabolism. Transferring yeast cells to sucrose medium activates Snf1, causing the phosphorylation of the transcriptional repressor Mig1, its translocation out of the nucleus and the derepression of *SUC2* [9, 10].

Snf1, like other kinases of the AMPK family, is activated by phosphorylation of a residue in its activation loop [11]. This involves one of 3 upstream kinases whose activity is, surprisingly, not regulated by glucose. Rather, evidence suggests that Snf1 activity is regulated by its dephosphorylation by the Protein Phosphatase

1 (PP1) complex made of the catalytic subunit, Glc7, and the glucose-specific regulatory subunit Reg1 [12]. How PP1 activity is linked to glucose availability is not yet clear, but deletion of *REG1* leads to constitutive Snf1 activity and to the expression of glucose-repressed genes even in the presence of glucose [13].

Another phenotype displayed by the *reg1Δ* strain is its ability to grow robustly in presence of 2DG [3, 14, 15]. This is attributed to the constitutive activation of Snf1 in this mutant, as mutations in *SNF1* cause hypersensitivity to 2DG and yeast lacking both Reg1 and Snf1 are also hypersensitive [16].

Despite the multifaceted cellular effects of 2DG, cells can indeed overcome 2DG toxicity by mechanisms that are currently being unraveled [reviewed in 3, 15]. A prolonged exposure of HeLa cells in 2DG-containing medium gave rise to resistant clones [17]. These cells displayed a high phosphatase activity towards 2DG-6-phosphate (2DG-6-P), suggesting the presence of an enzyme that could detoxify this metabolite back into 2DG and thus prevent the metabolic blockade. Studies in yeast also identified phosphatases, named Dog1 and Dog2, with a similar activity *in vitro* and whose overexpression allows growth in 2DG-containing medium [18, 19]. Recently, we found that the most abundant isoform, Dog2, is itself a glucose-repressed gene and thus is regulated by Snf1/AMPK function [20]. This partially explains why strains with high Snf1/AMPK activity are resistant to 2DG, such as *reg1Δ* [14, 16], other *reg1* mutant alleles [20, 21], a viable *glc7* mutation (Q48K) [21] or gain-of-function mutations in components of the AMPK complex [16, 21, 22]. However, additional resistance mechanisms independent of *DOG2* expression are at stake in these strains [20, 21]. This is suggested by the observation that *DOG2* deletion does not completely re-sensitize *reg1*Δ mutants to 2DG, and a point mutation in *REG1* (*reg1-P231L*) confers 2DG resistance but does not impact on the glucose-mediated repression of genes [21]. Thus, Snf1 likely controls additional factors participating in 2DG resistance.

One such candidate is the arrestin-related protein, Rod1. Arrestin-related proteins (ARTs) are important regulators of plasma membrane protein endocytosis in response to extracellular cues [23, 24]. ARTs recruit the ubiquitin ligase Rsp5 to nutrient transporters at the plasma membrane, promoting their subsequent ubiquitylation and endocytosis [25]. ART activity is regulated by nutrient signaling pathways, allowing to remodel the landscape of transporters at the plasma membrane to meet the physiological needs of cells facing a nutrient challenge [26, 27]. Particularly, Rod1 regulates endocytosis in response to glucose availability, and its activity is oppositely regulated by Snf1 and PP1 [28-30], being a direct target of Snf1 [31]. A genome-wide screen revealed that *rod1Δ* is indeed resistant to 2DG [14], thus the Snf1-mediated inhibition of Rod1 might contribute to 2DG resistance.

Point mutations aimed at abolishing Rod1 interaction with the ubiquitin ligase Rsp5, thereby annihilating their function as adaptor proteins in endocytosis, increased resistance to 2DG suggesting that it mediates 2DG toxicity through its function in endocytosis [32]. 2DG resistance of the *rod1Δ* strain is further increased by the

additional deletion of the *ROD1* paralogue *ROG3* [32]. Rod1 (and Rog3, to a lesser extent) controls the endocytosis of the glucose transporters Hxt1 and Hxt3 triggered in response to 2DG exposure, and overexpression of the same transporters in a *snf1Δ* mutant restored partial resistance to 2DG [32]. Deletion of *ROD1* and *ROG3* stabilized hexose transporters at the plasma membrane in *snf1Δ* and restored its 2DG-sensitivity to WT levels [32]. However, whether the effects of 2DG on endocytosis extend beyond glucose transporters is unknown, and there is currently no molecular understanding of how transporter stability/localization contributes to 2DG resistance.

In this study, we examined the effects of 2DG on endocytosis and found that 2DG triggers the endocytosis of many plasma membrane proteins, most of which depend on Rod1. Mechanistically, we show that opposite to the situation in mammalian cells, 2DG treatment leads to the dephosphorylation of Snf1/AMPK and several targets including Rod1, likely through a transient surge in PP1 activity. This favors Rod1 function and thus provides a rationale as to why this arrestin is central to 2DG-induced endocytosis. Finally, we demonstrate that 2DG resistance of the *rod1Δ* strain can solely be attributed to the maintenance of active glucose transporters at the membrane, where they can increase glucose uptake and contribute to detoxifying 2DG out of the cells, thus terminating the detoxification process.

Results

2DG triggers the endocytosis of many plasma membrane proteins

We previously described the proteomic changes occurring in response to 2DG and focused on proteins upregulated in this condition [20]. In addition, a few transmembrane/PM proteins displayed a significantly decreased abundance after 2h30 2DG treatment, including the amino acid permease Tat1 and the hexose transporter Hxt2 [20]. This could either be caused by a decreased synthesis or an active degradation by endocytosis. We verified this by looking at the regulation of the endogenously GFP-tagged proteins. Treatment of glucose-grown cells with 0.2% 2DG led to the degradation of PM-localized Tat1 and Hxt2 (**Fig 1A**), which was accompanied by their targeting to the vacuole (**Fig 1B**). Of note, we observed that the vacuole was strongly fragmented in response to 2DG (**Fig S1**), confirming recent findings [33]. This may be due to the fact that 2DG causes ER stress in yeast [20], which itself induces vacuolar fragmentation [34].

Tat2 and Hxt2 endocytosis in response to 2DG is reminiscent of the behavior of the low affinity hexose transporters Hxt1 and Hxt3 [32]. To document the extent of plasma membrane remodeling caused by 2DG exposure, we studied the regulation of a representative subset of plasma membrane proteins tagged with GFP at their endogenous loci before and after 2DG treatment. This included transporters of various substrates or structural classes, as well as receptor/sensor proteins whose expression could be detected in glucose-grown cells. This showed that many of these membrane proteins are endocytosed in response to 2DG (**Fig 1D, Fig S2**), implying that 2DG triggers a general endocytosis response.

In yeast, nutrient transporter endocytosis is driven by their ubiquitylation at the plasma membrane, which relies on the action of the ubiquitin ligase Rsp5 and adaptor proteins of the arrestin-like family (ARTs) [24, 27]. Previous work highlighted the importance of the arrestin-related protein Rod1 in the 2DG-induced endocytosis of Hxt1 and Hxt3 [32]. Indeed, we found that most of the cargoes studied here depended on Rod1 for their 2DG-induced endocytosis (**Fig 1D, Fig S2**). Although the Rod1 paralogue Rog3 displays some level of functional redundancy with Rod1 [32], Rog3 was not responsible for the endocytosis of the Rod1-independent cargo Lyp1 (**Fig S3**), although this may be the case for other cargoes. Altogether, these results indicate a prominent role for the ART protein Rod1 in 2DG-induced endocytosis.

2DG triggers endocytosis by inducing Rod1 dephosphorylation and ubiquitylation

We then focused on understanding why Rod1 function is so central for 2-deoxyglucose endocytosis. In the case of glucose-induced endocytosis, Rod1 activity is regulated through changes in its post-translational modifications [28, 29]. In a glucose-deprived medium, AMPK/Snf1 is active and phosphorylates Rod1, inhibiting its function [28, 29, 31, 35]. Conversely, glucose addition in the medium leads to Rod1 dephosphorylation in a

PP1-dependent manner, followed by its ubiquitylation by Rsp5 [28, 29]. These modifications promote its activity as an Rsp5 adaptor, leading to transporter ubiquitylation, endocytosis and vacuolar sorting [28, 29, 35]. Similarly, 2DG addition to glucose-grown cells triggers Rod1 ubiquitylation in an Rsp5- and PP1-dependent manner, but paradoxically 2DG was also reported to increase Snf1 activity [30, 32]. Thus, how 2DG regulates the relative activities of Snf1/PP1 and how this impacts on Rod1 activity are not fully understood.

Previously, the effect of 2DG on Rod1 post-translational modifications was evaluated using an 3HA-tagged construct [32]. Although Rod1-3HA could support the glucose-induced endocytosis of Jen1 [28], we realized that it was unable to restore the 2DG-induced endocytosis of Hxt1-GFP and Hxt3-GFP in a *rod1Δ* context , contrary to Flag-tagged Rod1 (Flag) which functionally behaved like the wild-type protein (**Fig S4A** and **B**). We then re-evaluated Rod1 post-translational modifications using this functional construct. As for Rod1-3HA [32], we observed drastic changes in Rod1 mobility on gel after 2DG treatment (**Fig 2A**). In glucose-grown cells, Rod1-Flag migrated as a diffuse band resulting from a mild phosphorylation, as determined by phosphatase treatment, and similarly to previously published results using Rod1-3HA [28, 32] (**Fig 2A**). This pattern gave rise to two discrete bands upon 2DG exposure, with the upper band corresponding to ubiquitylated Rod1, as shown by its disappearance when mutating the known ubiquitylated lysine(s) on Rod1 as described previously [28, 32]. The lower band corresponded to a dephosphorylated species of Rod1, as demonstrated by the fact that it migrated similarly as Rod1-Flag from phosphatase-treated extracts (**Fig 2B**). This fits with previous results obtained in the context of glucose-induced endocytosis, in which Rod1 ubiquitylation was preceded by its dephosphorylation [28, 29]. As expected, Rod1 was constitutively phosphorylated in the PP1 phosphatase mutant *reg1Δ* and this phosphorylation was no longer affected by 2DG treatment (**Fig 2B**). In contrast, mutations in the described Rod1 phosphatase, calcineurin (*cnb1*Δ) [36, 37] or in various signaling pathways whose activation is triggered by 2DG treatment [20] (MAPK= *slt2*Δ, *hog1*Δ; UPR: *hac1*Δ) had no impact (**Fig 2C**). This suggested that PP1 activity is required for the 2DG-induced dephosphorylation of Rod1. Moreover, deletion of *SNF1* or mutation of 12 serine residues within potential Snf1 consensus sequences [36] led to a profile comparable to that obtained in 2DG-treated cells, suggesting that lack of Rod1 phosphorylation mimics 2DG-treatment (**Fig 2D**).

Having confirmed how Rod1-Flag is post-translationally modified in response to 2DG, we assessed the functional consequences abrogating these modifications on the function of Rod1 in endocytosis. Instead of focusing on Hxt1 or Hxt3, which are glucose-regulated [32], we used Ina1-GFP as a model cargo (see **Fig 1D**). Ina1 is a protein of the SUR7/PalI family, with carries 3 predicted transmembrane domains and localizes to the plasma membrane [38]. Mutation of the ubiquitylation site(s) within Rod1 resulted in a slowdown of Ina1 endocytosis, whereas mutation of the PPxY motifs preventing the interaction with Rsp5 [28] completely

198 abolished it (Fig 2E). Growth assays demonstrate that Rod1 activity in endocytosis correlated with 2DG
199 sensitivity (Fig 2F). Interestingly, despite the fact that Rod1-S12A-Flag appeared constitutively
200 dephosphorylated/ubiquitylated (see Fig 2D), Ina1-GFP endocytosis still relied on 2DG addition, suggesting yet
201 another layer of regulation. Accordingly, Ina1 endocytosis was still regulated by 2DG in the *snf1Δ* mutant (Fig
202 2G), and so were other Rod1 cargoes (Fig S5). Thus, Rod1 dephosphorylation (or lack of phosphorylation) is
203 not sufficient to trigger endocytosis, suggesting yet an additional level of regulation.
204
205 **2DG promotes the PP1-dependent dephosphorylation of Snf1 and several of its targets**
206 The fact that 2DG triggers Rod1 dephosphorylation led us to think that this may occur through a transient
207 activation of PP1. Instead, 2DG was previously described to induce a mild phosphorylation (activation) of the
208 PP1 substrate Snf1 within 2h after treatment with 2DG [16], similar to observations in mammalian cells [3, 39].
209 To explain this discrepancy, we reexamined the effects of 2DG on Snf1 signaling. After 10 min 2DG treatment,
210 we never observed Snf1 activation, even at higher 2DG concentration (Fig 3A). On the contrary, 2DG
211 consistently decreased Snf1 phosphorylation within minutes after treatment (Fig 3B-C). A kinetic analysis of
212 phospho-Snf1 response to 2DG revealed a drop in Snf1 phosphorylation that is followed by an increase at later
213 time points (Fig 3B-C, 60' and 120'). Snf1 dephosphorylation by 2DG required the PP1 subunit Reg1, thus
214 mimicking the effect that glucose has on glucose-starved cells. Altogether, we conclude that 2DG triggers a
215 PP1-dependent dephosphorylation of Snf1, consistent with our (Fig 2) and others' [32] observations on Rod1.
216 This was further confirmed by studying another Snf1 substrate, the transcriptional repressor Mig1 [40,
217 41] which was also dephosphorylated after 2DG treatment in a PP1-dependent manner (Fig 3D). Again, this
218 mimicked the situation described when glucose-starved cells are treated with glucose [42]. Thus, 2DG triggers
219 both an immediate and transitory PP1-dependent inhibition of Snf1, and the direct or indirect
220 dephosphorylation of Snf1 substrates such as Mig1 or Rod1.
221
222 **Snf1 inactivation by 2DG requires 2DG phosphorylation by Hxk2**
223 We then investigated the origin of the signal triggering the PP1-dependent dephosphorylation of
224 substrates. 2DG is taken up by hexose transporters and is then phosphorylated into 2DG6P [43], which
225 interferes with several metabolic pathways. Hxk2 is the main hexokinase isoform expressed in glucose-grown
226 yeast cells [44] and we studied its contribution in 2DG phosphorylation by measuring 2DG6P appearance after
227 2DG treatment using an enzyme-based assay [45]. After 15 min exposure to 0.2% 2DG, 2DG6P was readily
228 detectable in WT cells (Fig 4A). In *hxk2Δ*, 2DG6P only reached 25% of the WT value (Fig 4A), suggesting that
229 Hxk2 is the main 2DG-phosphorylating enzyme.

2DG phosphorylation by hexokinase into the dead-end metabolite 2DG6P requires ATP and causes a strong ATP depletion [46, 47]. This can be visualized within minutes after 2DG addition in WT cells using an optimized, pH-insensitive version of the AT1.03 ATP FRET biosensor [48] (Fig 4B). The decrease in FRET signal occurred only upon 2DG treatment and revealed changes in ATP content as demonstrated using a mutant version of the FRET sensor which does not bind ATP [48] (Fig 4B). We found that comparatively to the WT, the drop in FRET was lower in *hxk2Δ* cells, again suggesting that Hxk2 is key for 2DG phosphorylation (Fig 4C).

In line with these findings, we found that neither Snf1 nor Rod1 were dephosphorylated in response to 2DG in the *hxk2Δ* mutant (Fig 4D). Similarly, 2DG no longer triggered Ina1-GFP endocytosis in these cells (Fig 4E). Overall, our data suggest that either Hxk2 itself or 2DG phosphorylation is required for the 2DG-mediated activation of PP1. Noteworthy, overexpression of the 2DG6P phosphatase Dog2, but not that of its catalytic-dead mutant (Dog2-DDAA), also abolished Ina1-GFP endocytosis (Fig 4F), suggesting that 2DG-6-P levels directly or indirectly control PP1 activity. Altogether, we propose that 2DG phosphorylation by Hxk2 triggers a transient activation of PP1, leading to Snf1 dephosphorylation, Rod1 dephosphorylation and endocytosis.

Stabilization of glucose transporters at the plasma membrane confers 2DG resistance to the *rod1Δ* mutant

So far, our data provide mechanistic insights as to how 2DG triggers endocytosis through PP1 and Rod1 activation. *ROD1* deletion leads to a partial 2DG resistance [14], but the underlying mechanism remains unclear. We previously described that a frequent strategy leading to 2DG resistance involves an increased expression of the Dog2 phosphatase at the transcriptional level [20]. However, using a *pDOG2*:LacZ reporter, we found that this was not the case in the *rod1*Δ mutant, suggesting a distinct mechanism (Fig 5A).

The 2DG resistance of the *rod1Δ* strain is exacerbated upon the further deletion of its paralogue *ROG3* [32], and other data indicate that 2DG resistance correlates with Rod1 activity in endocytosis [32] (see also Fig 2F). Since Rod1 has a central role in plasma membrane protein remodeling by 2DG (Fig 1D and Fig S2), we first hypothesized that the 2DG-mediated activation of Rod1 might trigger excessive endocytosis that would be deleterious for the cell, and could be counteracted by *ROD1* deletion. Importantly, deletion of the gene encoding the amphiphysin orthologue *RVS167,* involved in endocytosis, did not result in 2DG resistance (Fig 5B). Thus, it seems that only a partial endocytosis defect such as that observed in the *rod1Δ* (or *rod1Δ rog3Δ*) mutant causes 2DG resistance.

We postulated that 2DG resistance originates from the stabilization of one or several Rod1-regulated cargoes at the plasma membrane. We initially focused on the low affinity hexose transporters, Hxt1 and Hxt3, for the following reasons. First, the hypersensitivity of the *snf1Δ* mutant to 2DG is rescued by overexpression

of Hxt1 and Hxt3 through an unknown mechanism [32]. Second, duplication of a chromosomal region containing hexose transporter genes (*HXT3*, *HXT6* and *HXT7*) confers 2DG-resistance in a dominant manner [22]. Since these transporters are not endocytosed in the *rod1Δ* mutant (**Fig 1C** and **S2**) [32], we thus considered that their stabilization could contribute to 2DG resistance. Indeed, deletion of either *HXT3* or *HXT1* abolished the 2DG resistance of the *rod1Δ* mutant strain (**Fig 5C**), showing that both transporters are required for this process. In contrast, deletion of the high-affinity hexose transporter gene *HXT6* did not cause the same phenotype (**Fig 5C**). Although, it seems that only low-affinity hexose transporters promote 2DG resistance, this conclusion may be biased by the fact that low- and high-affinity hexose transporters are expressed to a lower level, the former contributing more to glucose uptake than the latter in glucose-rich conditions [49].

The growth defect of the obtained *rod1Δ hxt3Δ* strain on 2DG was restored by expressing a GFP-tagged version of Hxt3 driven by its own promoter on a low-copy (centromeric) plasmid (**Fig 5D**). This mild overexpression of Hxt3 also further increased 2DG resistance of the already resistant *rod1Δ* strain but had no effect on WT cells. Only a stronger expression of Hxt3 from a multicopy (2µ) plasmid conferred resistance to WT cells (**Fig 5E**), whereas that of Hxt1 had little or no effect as found previously [32]. Hxt1 and Hxt3 may have different functions regarding 2DG resistance, since Hxt1 overexpression did not compensate for the loss of Hxt3 in the *rod1Δ hxt3Δ* background (**Fig 5E**). Overall, we conclude that a high expression of glucose transporters generally correlates with 2DG resistance.

Structure/function studies of transporters [reviewed in 50] identified residues critical for hexose binding and translocation. In particular, residue N317 of the human glucose transporter GLUT1 binds glucose [51, 52] and mutation of the corresponding residue in yeast transporters alters substrate specificity and transport [53-55]. Particularly, mutation of this residue in Hxt1 (N370A) [56] and other yeast hexose transporters [53, 57] abolished glucose uptake. We mutated the corresponding residue in Hxt3 (N367A) and found that its overexpression no longer rescued growth on 2DG, further linking glucose transporter function with 2DG resistance (**Fig 5D**).

Stabilization of glucose transporters at the plasma membrane facilitates glucose uptake and 2DG export

The fact that glucose transport correlates with 2DG resistance was counterintuitive because 2DG enters into cells through glucose transporters [43], thus their stabilization at the cell surface may increase 2DG uptake. Indeed, deleting both *HXT1* and *HXT3* causes partial resistance to 2DG (**Fig 6A**), indicating that 2DG is mostly transported into cells through these transporters.

We considered two hypotheses to explain how glucose transporter accumulation at the plasma membrane results in 2DG resistance. First, by depleting glucose transporters from the plasma membrane, 2DG-

induced endocytosis could lower glucose intake at a time where glycolysis is already impacted, resulting in energy shortage as previously proposed [32]. Preventing endocytosis may therefore attenuate the glycolysis blockade by maintaining glucose uptake. Alternatively, transporters present at the cell surface may instead favor 2DG detoxification and release into the medium, as previously observed [43] since the directionality of transport (import or export) through hexose transporters is dictated by the concentration gradient.

We first tested whether *rod1Δ* cells could detoxify 2DG6P more efficiently than WT cells. Cells were treated for 2h with 2DG, and 2DG6P was generated at comparable levels in both strains (**Fig 6B**). Interestingly, the concentration of 2DG6P after 2h 2DG treatment was comparable to that observed after 15 min (**Fig 6C**), showing that saturation is reached very early after treatment. Cells were then transferred to a 2DG-free medium for 30 min and 2DG6P was assayed again. In both strains, 2DG6P concentration decreased during these 30 min, revealing they could detoxify 2DG6P (**Fig 6B**). However, the 2DG6P content was much lower in *rod1Δ* than in WT cells, suggesting that 2DG6P is better detoxified in this strain. Therefore, the endocytosis blockade caused by the deletion of *ROD1* allows a better detoxification of 2DG.

We also tested whether hexose transporters maintenance at the membrane impacts on glucose uptake, by using an intracellular glucose FRET sensor based on the bacterial glucose/galactose-binding transport protein MglB [58]. We assessed intracellular glucose following glucose exposure after a 4h-treatment with 2DG, and found that glucose accumulated slightly more in *rod1Δ* than in WT cells (**Fig 6E**). This depended on the presence of the glucose transporter Hxt3, since the additional deletion of *HXT3* in the context of *rod1Δ* restored glucose uptake to WT levels (**Fig 6E**) and 2DG sensitivity (**Fig 5C-E**). Finally, deletion of both *HXT1* and *HXT3* strongly impaired glucose uptake, as expected. Thus, *ROD1* deletion could facilitate cell survival independently of 2DG detoxification by allowing a sustained glucose uptake. This was further illustrated by the fact that deletion of *ROD1* conferred 2DG resistance to a strain lacking both *DOG1* and *DOG2*, that are central to 2DG detoxification (**Fig 6F**). Therefore, the lack of endocytosis of hexose transporters protects cells from 2DG toxicity by several mechanisms.

Discussion

Several strategies are known to modulate 2DG sensitivity/resistance in yeast [3]. The most common mechanism is through the aberrant activation of the AMPK orthologue, Snf1, either by gain-of-function mutation in constituents of the AMPK heterotrimeric complex, or by loss-of-function mutations of its inhibitory phosphatase (PP1: Glc7/Reg1) [3, 21]. How AMPK hyperactivation contributes to 2DG resistance is not fully understood, but we previously found that this partially occurs through the expression of the detoxification enzyme Dog2 [20]. Here, we provide important insights into the cellular effects that 2DG has on AMPK signaling, how this impacts Rod1 activity and subsequently, on endocytosis, and how endocytosis interference leads to 2DG resistance through the control of glucose transport activity.

We first report that 2DG acts as a strong endocytosis signal, leading to the endocytosis of many plasma membrane proteins. These include a GPCR (Ste2), various classes of transporters, such as permeases, solute carriers such as multidrug transporters of the major facilitator superfamily (MFS) or ATP-binding cassette (ABC) types. This massive 2DG-induced endocytosis of membrane proteins is reminiscent of that observed in other situations of metabolic stresses such as acute glucose or nitrogen starvation [59-61], or upon treatment with other drugs, stressors or heat shock [26, 62-67]. Because 2DG is an artificial molecule, the observed endocytosis is unlikely to originate from an adaptation strategy but rather informs us that 2DG-induced metabolic blockade triggers endocytosis through mechanisms that we further explored.

First, our work highlights the major role played by the arrestin Rod1 in 2DG-induced endocytosis. Rod1 participates in the endocytosis of the glucose transporters Hxt1 and Hxt3 upon 2DG treatment [32], and we extend these findings to many other membrane proteins. Using a tagged but fully functional protein, we confirm previous findings [32] that 2DG treatment strongly affects Rod1 post-translational modifications (phosphorylation and ubiquitylation), reminiscent of past studies focusing on the regulation of Rod1 by glucose availability [28, 29, 31, 36]. Phosphorylation is a frequent mechanism for arrestin inhibition [28, 63, 68, 69], perhaps by introducing negative charges that may hinder transporter interactions [61] [reviewed in 27]. Accordingly, Rod1 dephosphorylation and its subsequent ubiquitylation are required for its activity in endocytosis [28, 29]. Arrestin ubiquitylation is often required for their function [28, 68, 70], and this may favor interaction with Rsp5 and thus the Rsp5-mediated ubiquitylation of transporters [71]. Overall, we propose that 2DG induces an aberrant activation of Rod1 which explains the increased endocytosis observed in response to 2DG.

Second, we gained insights into how 2DG triggers these changes on Rod1, given that the precise effect of 2DG on Rod1 regulatory kinase(s) or phosphatase(s) was unclear until now. 2DG is well known to trigger AMPK

activation in mammalian cells even at short timepoints [3, 39, 72], and a similar but milder effect was reported for Snf1 in yeast after 2h treatment [16]. Yet, this apparent activation of Snf1 did not translate into an increased phosphorylation of its substrate Mig1 [16], and the reported dephosphorylation of Rod1 in these conditions was also not in line with an increased Snf1 activity. Rather, by focusing on shorter timepoints, we observed a sharp but transient decrease in Snf1 phosphorylation shortly after 2DG addition. Thus, 2DG treatment rapidly inhibits yeast Snf1 activity, contrary to observations on mammalian AMPK.

This inhibition likely occurred through an increased activity of its cognate phosphatase PP1 (Reg1/Glc7) [12, 73] (or increased accessibility of Snf1 to PP1). Accordingly, phosphorylation of the Snf1/PP1 target Mig1 also decreased in response to 2DG within a few minutes. Since Rod1 requires PP1 for dephosphorylation in response to glucose [28, 29] or 2DG [this study and 32], a sudden increase in PP1 activity in response to 2DG would also account for the changes in Rod1 post-translational modifications. The increased activity of PP1 in response to 2DG is reminiscent to that observed when glucose is added to cells deprived of glucose [74]. Thus, shortly after treatment and even in glucose-grown cells, 2DG treatment mimics glucose-replete conditions rather than starvation, and part of the early 2DG response involves a boost in PP1 activity.

The molecular mechanism by which PP1 is activated in these conditions is not yet clear. Despite a basal level of phosphorylation of Snf1 and Mig1 in glucose-grown cells, PP1 activity is already high in these conditions [12, 73], so how can 2DG further increase this activity? This apparent activation of PP1 by 2DG involves Hxk2, as 2DG was no longer able to trigger Snf1/Rod1 dephosphorylation or Ina1 endocytosis in the *hxk2Δ* strain. Hxk2 may either have a unique function in 2DG toxicity beyond its enzymatic function, but we favor the hypothesis that Hxk2 mediates 2DG-induced signaling through its unique ability to generate 2DG6P. Despite the fact that 2DG6P can be generated by other sugar-phosphorylating enzymes (Hxk1 and glucokinase Glk1) *in vitro* [21], only *HXK2* deletion causes 2DG resistance [14, 16, 20, 21]. Moreover, our *in vivo* data suggest that Hxk2 is the most prominent 2DG-phosphorylating enzyme, since *hxk2Δ* cells have a lower 2DG6P content and 2DG has a lower impact on the ATP status in these cells. The lack of effect of Hxk1 or Glk1 on 2DG toxicity could be explained by a lower expression level or other *in vivo* regulatory mechanisms that would prevent an efficient 2DG phosphorylation. Interestingly, both *HXK2* deletion and overexpression of the 2DG-6-P phosphatase Dog2, which converts 2DG-6-P back into 2DG, protect *snf1Δ* against 2DG hypersensitivity [16, 20], so both may act through a decreased 2DG6P content. More generally, 2DG has virtually no effect in strains overexpressing Dog2, further suggesting that 2DG6P (or a derived metabolite) contributes to the potential surge of PP1 activity. Further work should be aimed at understanding how the PP1/Snf1 balance is controlled by 2DG at the molecular level, which may help decipher the long-sought mechanism by which glucose-starved cells react to glucose addition [12, 74-76].

After delving into the mechanisms by which 2DG triggers endocytosis through the modulation of glucose signaling pathways and Rod1 activity, we also obtained insights into how *ROD1* deletion results in 2DG resistance. The study of Rod1 point mutants indicate a correlation between endocytosis and 2DG resistance [this work, and 32] and Hxt1 and Hxt3 stabilization at the plasma membrane was necessary for 2DG resistance, in line with the fact that their overexpression allows 2DG resistance [32]. Although Hxt1 and Hxt3 are the main transporters involved in 2DG uptake, their maintenance at the plasma membrane is required for long-term resistance through two possible pathways that possibly synergize (**Fig 7**). The first pathway involves 2DG detoxification. Indeed, 2DG triggers the induction of the Dog1 and Dog2 phosphatases which detoxicate 2DG6P into 2DG [20], the latter of which could presumably be exported once its cytosolic concentration is higher than that of the medium and provided that hexose transporters be present at the plasma membrane. This is in line with observations showing that (i) transport across the membrane is required to confer resistance, (ii) the same transport systems are used both for 2DG and glucose [43], and (iii) proteins of the GLUT/HXT family support bidirectional fluxes across the membrane [eg. GLUT2 in hepatocytes, reviewed in 77]. Accordingly, we found that *ROD1* deletion increases the ability to detoxify 2DG6P. The second pathway posits that transporter stabilization at the plasma membrane allows a sustained glucose import, and thus may help bypass the 2DG-induced glycolytic blockade. Over time, 2DG6P synthesis and accumulation should inhibit hexokinase and thus blocks glucose phosphorylation, which itself drives glucose import [78] [reviewed in 79], but given the existence of detoxification mechanisms, the glycolytic blockade may be only temporary. Increasing transporter availability should in principle boost glucose import and help glycolysis recover, and accordingly, *rod1Δ* cells contain more glucose than WT cells when exposed to glucose after 2DG treatment. Altogether, we propose that 2DG-induced endocytosis is detrimental to cells, and that deletion of *ROD1* partially corrects this by stabilizing glucose transporters, leading to a sustained glycolysis and 2DG export (**Fig 7**).

In mammalian cells, 2DG causes a fast energy depletion and AMPK activation [39]. This is exemplified by the opposite effect that 2DG has on the endocytosis of glucose transporters. In hepatocytes, the 2DG-induced activation of AMPK triggers the phosphorylation of the arrestin-like protein TXNIP, resulting in its degradation and stabilization of the glucose transporter GLUT1 [72], a response which is consistent with energy depletion and starvation response. In contrast, 2DG inhibits yeast Snf1, thus promoting Rod1-mediated glucose transporter endocytosis [this work and 32]. This somewhat paradoxical response likely reveals that in yeast, 2DG causes energy deprivation but is also likely sensed as excess glucose (causing a decreased Snf1/AMPK activity). The differences in 2DG signaling between these two model systems may originate from evolutionary differences regarding their ability to detect glucose as a signaling molecule, in addition to being a source of energy. Glucose is the preferred carbon source for *Saccharomyces cerevisiae* and is mostly used by

415 fermentation, implying a high glycolytic flux to sustain proliferation. Yeast has evolved various sensing systems
416 at the plasma membrane to detect extracellular glucose, that are wired into various signaling pathways [80].
417 It is likely that Hxk2 and/or glucose phosphorylation itself acts as a glucose sensor within the Snf1/AMPK
418 pathway [81-83], and 2DG phosphorylation by Hxk2 may produce a glucose-replete signal, leading to Snf1
419 inactivation despite changes in the energy load. This is probably only true shortly after 2DG treatment, before
420 2DG inhibits other aspects of cellular physiology (such as protein glycosylation or structural sugar metabolism)
421 leading to a complex response through stress-signaling pathway (such as UPR or MAPK-based signaling) [3,
422 20]. In conclusion, the characterization of 2DG resistance strategies led once more to a better understanding
423 of the cellular effects of 2DG and the diversity of mechanisms that can be deployed to bypass 2DG-induced
424 metabolic inhibition.
425

Materials and Methods

Yeast strain construction and growth conditions

All yeast strains used in this study derive from the *Saccharomyces cerevisiae* BY4741 or BY4742 background and are listed in table S1. Apart from the mutant strains obtained from the yeast deletion collection (Euroscarf) and the fluorescent GFP-tagged strains originating from the yeast GFP clone collection {Huh, 2003 #123}, all yeast strains were constructed by transformation with the standard lithium acetate–polyethylene glycol protocol using homologous recombination and verified by polymerase chain reaction (PCR) on genomic DNA prepared with a lithium acetate (200 mM)/SDS (0.1%) method (104). Yeast cells were grown in YPD medium (2%) or in SC medium [containing yeast nitrogen base (1.7 g/liter; MP Biomedicals), ammonium sulfate (5 g/liter; Sigma-Aldrich), the appropriate drop-out amino acid preparations (MP Biomedicals), and 2% (w/v) glucose, unless otherwise indicated]. Precultures were incubated at 30°C for 8 hours and diluted in the evening to 20-ml cultures to reach mid-log phase the next morning. 2DG (Sigma) was added to mid-log phase yeast cultures grown overnight to final concentrations of 0.2% (w/v) and incubated for the indicated times.

Plasmid construction

All plasmids used in this study are listed in table S2.

Plasmid pSL553 (pRS313, p_{ROD1}*:ROD1*-NcoI-Flag) was generated by site-directed mutagenesis on pSL234 (pRS313-based, p_{ROD1}*:ROD1*-Flag, a kind gift of O. Vincent, CSIC, Madrid, Spain) to integrate a NcoI site between *ROD1* and the Flag-tag, allowing to substitute the WT ORF of *ROD1* by mutated versions at SalI-NcoI sites as follows. The inserts p_{ROD1}*:ROD1*-WT-Flag (pSL559), p_{ROD1}*:ROD1-PYm*-Flag (pSL560) p_{ROD1}*:ROD1-S12A*-Flag (pSL561) and p_{ROD1}*:ROD1-KR*-Flag (pSL563) were PCR amplified (oSL1662/oSL1663) using as templates pSL94 (p_{ROD1}*:ROD1*-3HA) [28], pSL119 (p_{ROD1}*:ROD1-PYm*-3HA) [28], pSL152 (p_{ROD1}*:ROD1-S12A*-3HA) (unpublished, below), and pSL147 (p_{ROD1}*:ROD1-KR*-3HA) [28] respectively. They were digested with SalI/NcoI and cloned at these sites into pSL553 (p_{ROD1}*:ROD1*-NcoI-Flag). Plasmid pSL152 (pRS415, p_{ROD1}-ROD1(S12A)-3HA) was made from a synthetic gene designed to mutate S125, S138, S315, S358, S447, S623, S641, S706, S720, S734, S781, and S821 residues into A (Eurofins), digested PacI/XmaI and cloned PacI/XmaI into pSL94 at the place of WT *ROD1* (pRS415, p_{ROD1}*:ROD1*-3HA) [28].

To construct pSL589 (pUG35-based, p_{HXT3}-Hxt3-GFP), the *HXT3* promoter (1kb) was first cloned into pUG35 after amplification by PCR on WT gDNA (oSL1739/oSL1740) at BamHI/SpeI sites to give pSL592. The *HXT3-GFP* ORF was PCR-amplified (oSL1770/oSL1771) from gDNA of the Hxt3-GFP strain (ySL1027) using primers overlapping with the pSL592 sequence and cloned into pSL592 by gap-repair, and later rescued in bacteria to obtain pSL589. The N367A mutation was introduced using 2 overlapping PCR products amplified from gDNA of the HXT3-GFP strain (ySL1027) (oSL1730/oSL682 and oSL1731/oSL1563) and cloned by gap-repair into pSL592 to give pSL591. Plasmid pSL599 (pRS426, p_{HXT1}*:HXT1*) was obtained by (1) amplifying the *HXT1* gene (-515/+225) from WT genomic DNA (oSL435/oSL932) into a pCRII-blunt topo vector (pSL597), (2) cloning a BamHI/XhoI fragment of pSL597 into pRS425 at BamHI/XhoI sites. For plasmid pSL602 (pRS426, p_{HXT1}*:HXT1*), A PCR amplifying the *HXT3* gene (and 1kb of promoter) was obtained from WT genomic DNA (oSL1739/oSL1734), digested BamhI/SpeI and cloned BamHI/SpeI in pRS426.

All constructs were verified by sequencing.

Total protein extracts and immunoblotting

Yeast were always grown in SC medium. For each protein sample, 1.4 ml of culture was incubated with 140µl of 100% TCA for 10 min on ice to precipitate proteins, centrifuged at 16,000g at 4°C for 10 min, and broken for 10 min with glass beads. Lysates were transferred to another 1.5-ml tube to remove glass beads and centrifuged for 5 min at 16,000g at 4°C, supernatants were discarded, and protein pellets were resuspended in sample buffer [50 mM tris-HCl (pH 6.8), 100 mM dithiothreitol, 2% SDS, 0.1% bromophenol blue, and 10% glycerol, complemented with 50 mM tris-base (pH 8.8)] (50µl/initial OD). Protein samples were heated at 37°C

for 5 min and 10 µl was loaded on SDS–polyacrylamide gel electrophoresis (PAGE) gels (4-20% Mini-PROTEAN TGX Stain-Free, Bio-Rad). After electrophoresis for 30 min at 200V, total proteins were visualized by in-gel fluorescence using a trihalo compound incorporated in SDS–PAGE gels (stain-free TGX gels, 4–20%; Bio-Rad) after 45 sec UV-induced photoactivation using a ChemiDoc MP imager (BioRad), serving as a loading control. Gels were transferred on nitrocellulose membranes for 60 min (100V) in a liquid transfer system (Bio-Rad). Membranes were blocked in Tris-buffered saline solution containing 0.5% Tween-20 (TBS-T) and 2% milk for 30 min and incubated for at least 2 hours with the corresponding primary antibodies. Membranes were washed 3x10 min in TBS-T and incubated for at least an hour with the corresponding secondary antibody (coupled with horseradish peroxidase). Membranes were then washed again 3x10 min in TBS-T and incubated with SuperSignal™ West Femto reagent (Thermo). Luminescence signals were acquired using a ChemiDoc MP (BioRad). Primary and secondary antibodies used in this study as well as their dilutions are listed in table S3.

Treatment of protein extracts with calf intestinal phosphatase (CIP)

Calf Intestine Phosphatase (CIP, Roche ref 11097075001) was used to dephosphorylate proteins prior to electrophoresis. Samples were prepared using 20 µL of TCA protein extract (see "Protein extracts and immunoblotting", above), to which 2 µL of 10X CIP buffer supplied with the enzyme, as well as 0.6 µL of 1.5M Tris pH 8.8, 0.2 µL 0.1M $MgSO_4$, and 17.2 µL of H_2O were added. The extract was split in 2 and 0.6 U CIP was added to one of the samples. Samples were incubated at 37°C for 3 h, and loaded on SDS-PAGE.

Purification of Ina1-GFP for ubiquitylation analysis

Strains expressing Ina1-GFP were transformed with an empty plasmid or a plasmid containing 6xHis-tagged ubiquitin under the control of the promoter of the copper-inducible *CUP1* gene (pSL205). Ubiquitylation analysis was performed as described before [84]. Briefly, cells were grown to the exponential phase before induction with 100µM $CuS0_4$, with or without 2DG 0.2%, for 1h at 30°C. Around 20 OD of cells were centrifuged at 4,000 g for 5 minutes, the pellets were washed with cold water and resuspended with 200µl of RIPA buffer (50 mM TRIS /HCl pH 7.5. 150 mM NaCl. 0,1% SDS, 2 mM EDTA, 50 mM NaF, 1% NP-40, 0,5% Na-Deoxycholate, 1% Glycerol) supplemented with protease inhibitor (Complete EDTA-free, Roche), 1mM PMSF (Sigma), 10mM NEM (Sigma) and 0.1mM MG-132 (Enzo Life Sciences) and broken with glass beads for 8 min at 4°C. Lysates were then rotated at 4°C for 15 minutes and centrifuged at 10,000g for 10 min at 4°C. 10µl of GFP-Trap agarose-magnetic beads (Chromotek) were added to the lysates and rotated overnight at 4°C. After 2 washes with 1.5 mL of wash buffer (50 mM TRIS /HCl pH 7.5, 150 mM NaCl, 1% NP-40, 5% Glycerol) at 4°C and 1 wash with 1.5mL TBST 0.1% at RT, the beads were resuspended with 25µl of boiling buffer (50 mM TRIS, pH =7,5, 1 mM EDTA, 1% SDS, 20% Glycerol) and incubated at 37°C for 30 minutes. 25µl of Urea SDS buffer (150mM TRIS, pH =6.8, 6M Urea, 6% SDS, bromophenol blue) were added and the proteins were incubated for another 30 minutes at 37°C before loading on a 4-12% SDS-PAGE (Mini-PROTEAN TGX Stain-Free, Bio-Rad).

Beta-galactosidase assays

Beta-galactosidase assays were performed using 1 ml of mid-log phase yeast cultures carrying the *pDOG1-LacZ* (pSL409) or *pDOG2-LacZ* plasmids (pSL410) [20], grown overnight to the mid-log phase in SC medium without uracil with 2% glucose and switched to the specified conditions. The OD(600 nm) of the culture was measured, and samples were taken and centrifuged at 16,000g at 4°C for 10 min. Cell pellets were snap-frozen in liquid nitrogen and resuspended in 800 µl of buffer Z (pH 7, 50 mM NaH_2PO_4, 45 mM Na_2HPO_4, 10 mM $MgSO_4$, 10 mM KCl, and 38 mM beta-mercaptoethanol). After addition of 160µl of ONPG (ortho-nitrophenyl-d-galactopyranoside, 4 mg/ml; Sigma-Aldrich), samples were incubated at 37°C. Enzymatic reactions were stopped in the linear phase (60-min incubation for *pDOG2-LacZ* and 120-min incubation for the *pDOG1-LacZ* plasmid, as per initial tests) [20] by addition of 400 µl of Na_2CO_3, and cell debris were discarded by centrifugation at 16,000g. The absorbance of clarified samples was measured with a spectrophotometer set at 420 nm.

Galactosidase activities (arbitrary units) were calculated using the formula 1000*[A420/(A600*t)], where A420 refers to the measured enzyme activity, A600 is the turbidity of the culture, and t is the incubation time. Each enzymatic assay was repeated independently at least three times.

2DG-6-phosphate assays

Cells were grown overnight in SC media until mid-log phase. 2DG was added into the culture to a final concentration of 0.2% for the indicated time. For the chase experiments, the cultures were centrifuged after 2 hours, washed with water and re-suspended in the same volume of SC medium without 2DG. For each time points, 1 OD equivalent of cells were taken, immediately placed on ice, centrifuged at 4°C for 4' at 16,000g, washed once with cold PBS and lysed using Y-PER™ Yeast Protein Extraction Reagent (ThermoFisher Scientific) as previously described [85]. Briefly, 1 OD equivalent of cells was resuspended in 100µL of Y-PER buffer, incubated for 20' at 30°C, and centrifuged for 4' at 16100g at room temperature. The supernatant (between 0.0125 and 0.0625 OD equivalents) was used for the assay and diluted in Y-PER when needed. The assay was performed using the 2DG uptake measurement kit (Cosmo Bio USA, Carlsbad, CA, USA;, Ref. CSR-OKP-PMG-K01H) following the manufacturer's protocol adapted for a total reaction volume of 100 µL. Absorbance at 420 nm was measured every minute for 1 hour on a SpectraMax® M2 Microplate Reader (Molecular Devices). Measures taken between 20 and 35 minutes (linear range) were taken into account to compare the slopes. Each sample was assayed at least twice in each experiment and at least three independent experiments were performed. Mean values were calculated and were plotted with error bars representing SEM. Statistical significance was determined using a *t*-test for paired variables assuming a normal distribution of the values, as follows: *P ≤ 0.05, **P ≤ 0.01, ***P ≤ 0.001; ns, P > 0.05 using GraphPad Prism7.

Glucose FRET sensor experiments

Yeast transformed with the plasmid FLII12Pglu-700µδ6 (pSL590, [a gift from Wolf Frommer: Addgene #28002, 58] were grown overnight in SC-URA medium to reach an OD600nm of 0.3-0.7 in the morning. Cells were centrifuged at 3000g for 5 minutes and the cell pellets were resuspended in 20mM MES pH=6 to a final OD of 0.6. 180µl of the cell suspension were distributed in 12 wells of a 96-well black PS microplate with flat bottom (Greiner). Fluorescence was measured with a plate reader (Spark, TECAN) set at 30°C before the experiment was started.

A first measurement for 3 cycles was performed to establish a baseline (each cycle is around 90 seconds with 10 seconds shaking before each measurement of the fluorescence). Cells were excited at CFP wavelength excitation (428 nm) and the emission intensities at 485 nm (CFP) and 528 nm (Citrine) were collected. The cycle was then paused to inject 20µl of the glucose solutions using a multichannel pipette, and the plate rapidly reloaded in the reader to restart measurements for another 17 cycles. Data were collected and analyzed in an Excel spreadsheet and in Prism 7.0 (GraphPad). Emission intensity values of yeast transformed with an empty plasmid were subtracted from emissions values at 485 nm and 528 nm for each measurement at the different glucose concentrations. The emission intensity ratio for Citrine (528 nm) over CFP (485 nm) was calculated. All analyses were repeated (with three technical replicates) at least three times independently. Emission ratios were normalized to the average of the three initial ratio values before glucose addition.

ATP FRET sensor experiments

Yeast transformed with the plasmid pDRF1-GW yAT1.03 (pSL608) [a gift from Bas Teusink: Addgene #132781, 48] were grown overnight in SC-URA medium to reach an OD600nm of 0.3-0.7 in the morning. FRET measurements were performed as above except cells were excited at 438 nm and the emission intensities at 483 nm (ymTq2Δ11) and 593nm (tdTomato) were collected. A plasmid encoding a mutated sensor which does not bind ATP (pSL609) [a gift from Bas Teusink: Addgene #132782, 48] was used as a negative control.

Drop tests

Yeast cells grown in liquid-rich or SC medium for at least 6 hours at 30°C were adjusted to an optical density (600 nm) of 1. Serial 10-fold dilutions were prepared in 96-well plates and spotted on plates containing rich or SC medium containing 2% (w/v) agar and, when indicated, 2DG [0.05 or 0.2% (w/v)]. Plates were incubated at 30°C for 3 to 4 days before scanning on a desktop scanner (Epson).

Microscopy

Cells were mounted in synthetic complete medium with the appropriate carbon source and observed with a motorized Olympus BX-61 fluorescence microscope equipped with an Olympus PlanApo 100× oil-immersion objective (1.40 NA), a Spot 4.05 charge-coupled device camera and the MetaVue acquisition software (Molecular Devices; Sunnyvale, CA) and imaged at room temperature. GFP-tagged proteins were visualized using a Chroma GFP II filter (excitation 440–470 nm). mCherry-tagged proteins were visualized using an HcRed I filter (excitation 525–575 nm). Images were processed in ImageJ (NIH). Vacuolar staining was obtained by incubating cells grown in the desired condition with 100 µM CMAC (Life Technologies) for 10 min under agitation at 30°C. Cells are then washed twice with water before observations with a fluorescence microscope equipped with a DAPI filter.

Quantification of vacuolar fragmentation

Quantification of vacuolar fragmentation (Fig. S1B) was performed with ImageJ. For each experiment and each strain, at least 30 cells were observed and the quantification was done blindly. Cells with more than 3 vacuoles were considered as cells with highly fragmented vacuoles.

Quantification of Western-blots

Western blot quantifications were performed with ImageJ. The integrated density of proteins of interest was divided by the integrated density of total proteins. Results were normalized to the Glc ON condition of each protein. The ratio of undegraded protein is shown. The experiments were repeated three times. Datas were analyzed and processed with Prism7 software (GraphPad). The statistical test performed was a one-way analysis of variance (ANOVA) test. *: 0.01<P-value<0.05; **: 0.001<P-value<0.01; ***: 0.0001<P-value<0.001; ****: P-value<0.0001.

Statistical analysis

Mean values were calculated using a minimum of three independent measurements from three biological replicates and were plotted with error bars representing SEM. Statistical significance was determined using a *t*-test for paired variables assuming a normal distribution of the values, as follows: *P ≤ 0.05, **P ≤ 0.01, ***P ≤ 0.001; ns, P > 0.05 using GraphPad Prism7.

References

1. Xi H, Kurtoglu M, Lampidis TJ. The wonders of 2-deoxy-D-glucose. IUBMB Life. 2014;66(2):110-21. Epub 2014/03/01. doi: 10.1002/iub.1251. PubMed PMID: 24578297.
2. Hardie DG. Regulation of AMP-activated protein kinase by natural and synthetic activators. Acta Pharm Sin B. 2016;6(1):1-19. doi: 10.1016/j.apsb.2015.06.002. PubMed PMID: 26904394; PubMed Central PMCID: PMCPMC4724661.
3. Laussel C, Leon S. Cellular toxicity of the metabolic inhibitor 2-deoxyglucose and associated resistance mechanisms. Biochem Pharmacol. 2020;182:114213. doi: 10.1016/j.bcp.2020.114213. PubMed PMID: 32890467.
4. Kurtoglu M, Gao N, Shang J, Maher JC, Lehrman MA, Wangpaichitr M, et al. Under normoxia, 2-deoxy-D-glucose elicits cell death in select tumor types not by inhibition of glycolysis but by interfering with N-linked glycosylation. Molecular cancer therapeutics. 2007;6(11):3049-58. Epub 2007/11/21. doi: 10.1158/1535-7163.MCT-07-0310. PubMed PMID: 18025288.
5. Luengo A, Gui DY, Vander Heiden MG. Targeting Metabolism for Cancer Therapy. Cell Chem Biol. 2017;24(9):1161-80. doi: 10.1016/j.chembiol.2017.08.028. PubMed PMID: 28938091; PubMed Central PMCID: PMCPMC5744685.
6. Pajak B, Siwiak E, Soltyka M, Priebe A, Zielinski R, Fokt I, et al. 2-Deoxy-d-Glucose and Its Analogs: From Diagnostic to Therapeutic Agents. Int J Mol Sci. 2019;21(1). doi: 10.3390/ijms21010234. PubMed PMID: 31905745; PubMed Central PMCID: PMCPMC6982256.
7. Kayikci O, Nielsen J. Glucose repression in Saccharomyces cerevisiae. FEMS Yeast Res. 2015;15(6):fov068. doi: 10.1093/femsyr/fov068. PubMed PMID: 26205245; PubMed Central PMCID: PMCPMC4629793.
8. Coccetti P, Nicastro R, Tripodi F. Conventional and emerging roles of the energy sensor Snf1/AMPK in Saccharomyces cerevisiae. Microb Cell. 2018;5(11):482-94. doi: 10.15698/mic2018.11.655. PubMed PMID: 30483520; PubMed Central PMCID: PMCPMC6244292.
9. De Vit MJ, Waddle JA, Johnston M. Regulated nuclear translocation of the Mig1 glucose repressor. Molecular Biology of the Cell. 1997;8(8):1603-18. PubMed PMID: 9285828; PubMed Central PMCID: PMCPMC276179.
10. Papamichos-Chronakis M, Gligoris T, Tzamarias D. The Snf1 kinase controls glucose repression in yeast by modulating interactions between the Mig1 repressor and the Cyc8-Tup1 co-repressor. EMBO Rep. 2004;5(4):368-72. doi: 10.1038/sj.embor.7400120. PubMed PMID: 15031717; PubMed Central PMCID: PMCPMC1299031.
11. McCartney RR, Schmidt MC. Regulation of Snf1 kinase. Activation requires phosphorylation of threonine 210 by an upstream kinase as well as a distinct step mediated by the Snf4 subunit. The Journal of biological chemistry. 2001;276(39):36460-6. doi: 10.1074/jbc.M104418200. PubMed PMID: 11486005.
12. Rubenstein EM, McCartney RR, Zhang C, Shokat KM, Shirra MK, Arndt KM, et al. Access denied: Snf1 activation loop phosphorylation is controlled by availability of the phosphorylated threonine 210 to the PP1 phosphatase. J Biol Chem. 2008;283(1):222-30. Epub 2007/11/10. doi: 10.1074/jbc.M707957200. PubMed PMID: 17991748.
13. Tu J, Carlson M. REG1 binds to protein phosphatase type 1 and regulates glucose repression in Saccharomyces cerevisiae. EMBO J. 1995;14(23):5939-46. Epub 1995/12/01. PubMed PMID: 8846786; PubMed Central PMCID: PMCPMC394713.
14. Ralser M, Wamelink MM, Struys EA, Joppich C, Krobitsch S, Jakobs C, et al. A catabolic block does not sufficiently explain how 2-deoxy-D-glucose inhibits cell growth. Proc Natl Acad Sci U S A. 2008;105(46):17807-11. doi: 10.1073/pnas.0803090105. PubMed PMID: 19004802; PubMed Central PMCID: PMC2584745.
15. Schmidt MC, O'Donnell AF. 'Sugarcoating' 2-deoxyglucose: mechanisms that suppress its toxic effects. Current genetics. 2021;67(1):107-14. doi: 10.1007/s00294-020-01122-7. PubMed PMID: 33136227.
16. McCartney RR, Chandrashekarappa DG, Zhang BB, Schmidt MC. Genetic analysis of resistance and sensitivity to 2-deoxyglucose in Saccharomyces cerevisiae. Genetics. 2014;198(2):635-46. doi: 10.1534/genetics.114.169060. PubMed PMID: 25116136; PubMed Central PMCID: PMC4196618.
17. Barban S. Studies on the mechanism of resistance to 2-deoxy-D-glucose in mammalian cell cultures. J Biol Chem. 1962;237:291-5. Epub 1962/02/01. PubMed PMID: 13864809.
18. Sanz P, Randez-Gil F, Prieto JA. Molecular characterization of a gene that confers 2-deoxyglucose resistance in yeast. Yeast. 1994;10(9):1195-202. Epub 1994/09/01. doi: 10.1002/yea.320100907. PubMed PMID: 7754708.
19. Randez-Gil F, Blasco A, Prieto JA, Sanz P. DOGR1 and DOGR2: two genes from Saccharomyces cerevisiae that confer 2-deoxyglucose resistance when overexpressed. Yeast. 1995;11(13):1233-40. Epub 1995/10/01. doi: 10.1002/yea.320111303. PubMed PMID: 8553694.

20. Defenouillère Q, Verraes A, Laussel C, Friedrich A, Schacherer J, Leon S. The induction of HAD-like phosphatases by multiple signaling pathways confers resistance to the metabolic inhibitor 2-deoxyglucose. Sci Signal. 2019;12(597):aaw8000. doi: 10.1126/scisignal.aaw8000. PubMed PMID: 31481524.
21. Soncini SR, Chandrashekarappa DG, Augustine DA, Callahan KP, O'Donnell AF, Schmidt MC. Spontaneous mutations that confer resistance to 2-deoxyglucose act through Hxk2 and Snf1 pathways to regulate gene expression and HXT endocytosis. PLoS Genet. 2020;16(7):e1008484. doi: 10.1371/journal.pgen.1008484. PubMed PMID: 32673313; PubMed Central PMCID: PMCPMC7386655.
22. Barney JB, Chandrashekarappa DG, Soncini SR, Schmidt MC. Drug resistance in diploid yeast is acquired through dominant alleles, haploinsufficiency, gene duplication and aneuploidy. PLoS Genet. 2021;17(9):e1009800. doi: 10.1371/journal.pgen.1009800. PubMed PMID: 34555030; PubMed Central PMCID: PMCPMC8460028.
23. Piper RC, Dikic I, Lukacs GL. Ubiquitin-dependent sorting in endocytosis. Cold Spring Harb Perspect Biol. 2014;6(1). Epub 2014/01/05. doi: 10.1101/cshperspect.a016808. PubMed PMID: 24384571; PubMed Central PMCID: PMCPMC3941215.
24. MacGurn JA, Hsu PC, Emr SD. Ubiquitin and membrane protein turnover: from cradle to grave. Annu Rev Biochem. 2012;81:231-59. Epub 2012/03/13. doi: 10.1146/annurev-biochem-060210-093619. PubMed PMID: 22404628.
25. Sardana R, Emr SD. Membrane Protein Quality Control Mechanisms in the Endo-Lysosome System. Trends Cell Biol. 2021;31(4):269-83. doi: 10.1016/j.tcb.2020.11.011. PubMed PMID: 33414051.
26. Babst M. Regulation of nutrient transporters by metabolic and environmental stresses. Curr Opin Cell Biol. 2020;65:35-41. doi: 10.1016/j.ceb.2020.02.009. PubMed PMID: 32200208; PubMed Central PMCID: PMCPMC7501145.
27. Kahlhofer J, Leon S, Teis D, Schmidt O. The alpha-arrestin family of ubiquitin ligase adaptors links metabolism with selective endocytosis. Biology of the cell / under the auspices of the European Cell Biology Organization. 2021;113(4):183-219. Epub 2020/12/15. doi: 10.1111/boc.202000137. PubMed PMID: 33314196.
28. Becuwe M, Vieira N, Lara D, Gomes-Rezende J, Soares-Cunha C, Casal M, et al. A molecular switch on an arrestin-like protein relays glucose signaling to transporter endocytosis. J Cell Biol. 2012;196(2):247-59. Epub 2012/01/18. doi: 10.1083/jcb.201109113. PubMed PMID: 22249293.
29. Llopis-Torregrosa V, Ferri-Blazquez A, Adam-Artigues A, Deffontaines E, van Heusden GP, Yenush L. Regulation of the Yeast Hxt6 Hexose Transporter by the Rod1 alpha-Arrestin, the Snf1 Protein Kinase, and the Bmh2 14-3-3 Protein. J Biol Chem. 2016;291(29):14973-85. doi: 10.1074/jbc.M116.733923. PubMed PMID: 27261460; PubMed Central PMCID: PMC4946916.
30. O'Donnell AF, Schmidt MC. AMPK-Mediated Regulation of Alpha-Arrestins and Protein Trafficking. Int J Mol Sci. 2019;20(3). Epub 2019/01/30. doi: 10.3390/ijms20030515. PubMed PMID: 30691068; PubMed Central PMCID: PMCPMC6387238.
31. Shinoda J, Kikuchi Y. Rod1, an arrestin-related protein, is phosphorylated by Snf1-kinase in *Saccharomyces cerevisiae*. Biochem Biophys Res Commun. 2007;364(2):258-63. Epub 2007/10/24. doi: 10.1016/j.bbrc.2007.09.134. PubMed PMID: 17949685.
32. O'Donnell AF, McCartney RR, Chandrashekarappa DG, Zhang BB, Thorner J, Schmidt MC. 2-Deoxyglucose impairs *Saccharomyces cerevisiae* growth by stimulating Snf1-regulated and alpha-arrestin-mediated trafficking of hexose transporters 1 and 3. Mol Cell Biol. 2015;35(6):939-55. doi: 10.1128/MCB.01183-14. PubMed PMID: 25547292; PubMed Central PMCID: PMCPMC4333089.
33. Yang X, Reist L, Chomchai DA, Chen L, Arines FM, Li M. ESCRT, not intralumenal fragments, sorts ubiquitinated vacuole membrane proteins for degradation. J Cell Biol. 2021;220(8). doi: 10.1083/jcb.202012104. PubMed PMID: 34047770; PubMed Central PMCID: PMCPMC8167898.
34. Stauffer B, Powers T. Target of rapamycin signaling mediates vacuolar fission caused by endoplasmic reticulum stress in Saccharomyces cerevisiae. Mol Biol Cell. 2015;26(25):4618-30. Epub 2015/10/16. doi: 10.1091/mbc.E15-06-0344. PubMed PMID: 26466677; PubMed Central PMCID: PMCPMC4678019.
35. Becuwe M, Leon S. Integrated control of transporter endocytosis and recycling by the arrestin-related protein Rod1 and the ubiquitin ligase Rsp5. eLife. 2014;3:03307. doi: 10.7554/eLife.03307. PubMed PMID: 25380227; PubMed Central PMCID: PMC4244573.
36. Alvaro CG, Aindow A, Thorner J. Differential Phosphorylation Provides a Switch to Control How alpha-Arrestin Rod1 Down-regulates Mating Pheromone Response in Saccharomyces cerevisiae. Genetics. 2016;203(1):299-317. Epub 2016/02/28. doi: 10.1534/genetics.115.186122. PubMed PMID: 26920760; PubMed Central PMCID: PMCPMC4858781.

37. Alvaro CG, O'Donnell AF, Prosser DC, Augustine AA, Goldman A, Brodsky JL, et al. Specific alpha-arrestins negatively regulate *Saccharomyces cerevisiae* pheromone response by down-modulating the G-protein-coupled receptor Ste2. Mol Cell Biol. 2014;34(14):2660-81. doi: 10.1128/MCB.00230-14. PubMed PMID: 24820415; PubMed Central PMCID: PMCPMC4097657.
38. Germann SM, Schramke V, Pedersen RT, Gallina I, Eckert-Boulet N, Oestergaard VH, et al. TopBP1/Dpb11 binds DNA anaphase bridges to prevent genome instability. J Cell Biol. 2014;204(1):45-59. doi: 10.1083/jcb.201305157. PubMed PMID: 24379413; PubMed Central PMCID: PMCPMC3882784.
39. Vincent EE, Coelho PP, Blagih J, Griss T, Viollet B, Jones RG. Differential effects of AMPK agonists on cell growth and metabolism. Oncogene. 2015;34(28):3627-39. doi: 10.1038/onc.2014.301. PubMed PMID: 25241895; PubMed Central PMCID: PMCPMC4980123.
40. Smith FC, Davies SP, Wilson WA, Carling D, Hardie DG. The SNF1 kinase complex from Saccharomyces cerevisiae phosphorylates the transcriptional repressor protein Mig1p in vitro at four sites within or near regulatory domain 1. FEBS Lett. 1999;453(1-2):219-23. doi: 10.1016/s0014-5793(99)00725-5. PubMed PMID: 10403407.
41. Treitel MA, Kuchin S, Carlson M. Snf1 protein kinase regulates phosphorylation of the Mig1 repressor in Saccharomyces cerevisiae. Mol Cell Biol. 1998;18(11):6273-80. Epub 1998/10/17. PubMed PMID: 9774644; PubMed Central PMCID: PMCPMC109214.
42. Shashkova S, Wollman AJM, Leake MC, Hohmann S. The yeast Mig1 transcriptional repressor is dephosphorylated by glucose-dependent and -independent mechanisms. FEMS Microbiol Lett. 2017;364(14). Epub 2017/09/01. doi: 10.1093/femsle/fnx133. PubMed PMID: 28854669.
43. van Steveninck J. Transport-associated phosphorylation of 2-deoxy-D-glucose in yeast. Biochim Biophys Acta. 1968;163(3):386-94. Epub 1968/11/05. doi: 10.1016/0005-2736(68)90123-5. PubMed PMID: 5721900.
44. Herrero P, Galindez J, Ruiz N, Martinez-Campa C, Moreno F. Transcriptional regulation of the Saccharomyces cerevisiae HXK1, HXK2 and GLK1 genes. Yeast. 1995;11(2):137-44. doi: 10.1002/yea.320110205. PubMed PMID: 7732723.
45. Saito K, Lee S, Shiuchi T, Toda C, Kamijo M, Inagaki-Ohara K, et al. An enzymatic photometric assay for 2-deoxyglucose uptake in insulin-responsive tissues and 3T3-L1 adipocytes. Anal Biochem. 2011;412(1):9-17. doi: 10.1016/j.ab.2011.01.022. PubMed PMID: 21262191.
46. Karczmar GS, Arbeit JM, Toy BJ, Speder A, Weiner MW. Selective depletion of tumor ATP by 2-deoxyglucose and insulin, detected by 31P magnetic resonance spectroscopy. Cancer Res. 1992;52(1):71-6. Epub 1992/01/01. PubMed PMID: 1727388.
47. Ibanez AJ, Fagerer SR, Schmidt AM, Urban PL, Jefimovs K, Geiger P, et al. Mass spectrometry-based metabolomics of single yeast cells. Proc Natl Acad Sci U S A. 2013;110(22):8790-4. doi: 10.1073/pnas.1209302110. PubMed PMID: 23671112; PubMed Central PMCID: PMCPMC3670324.
48. Botman D, van Heerden JH, Teusink B. An Improved ATP FRET Sensor For Yeast Shows Heterogeneity During Nutrient Transitions. ACS Sens. 2020;5(3):814-22. doi: 10.1021/acssensors.9b02475. PubMed PMID: 32077276; PubMed Central PMCID: PMCPMC7106129.
49. Ozcan S, Johnston M. Function and regulation of yeast hexose transporters. Microbiol Mol Biol Rev. 1999;63(3):554-69. doi: 10.1042/bj3630737. PubMed PMID: 10477308; PubMed Central PMCID: PMCPMC103746.
50. Yan N. A Glimpse of Membrane Transport through Structures-Advances in the Structural Biology of the GLUT Glucose Transporters. J Mol Biol. 2017;429(17):2710-25. doi: 10.1016/j.jmb.2017.07.009. PubMed PMID: 28756087.
51. Mueckler M, Makepeace C. Model of the exofacial substrate-binding site and helical folding of the human Glut1 glucose transporter based on scanning mutagenesis. Biochemistry. 2009;48(25):5934-42. doi: 10.1021/bi900521n. PubMed PMID: 19449892; PubMed Central PMCID: PMCPMC2776625.
52. Deng D, Xu C, Sun P, Wu J, Yan C, Hu M, et al. Crystal structure of the human glucose transporter GLUT1. Nature. 2014;510(7503):121-5. doi: 10.1038/nature13306. PubMed PMID: 24847886.
53. Farwick A, Bruder S, Schadeweg V, Oreb M, Boles E. Engineering of yeast hexose transporters to transport D-xylose without inhibition by D-glucose. Proc Natl Acad Sci U S A. 2014;111(14):5159-64. doi: 10.1073/pnas.1323464111. PubMed PMID: 24706835; PubMed Central PMCID: PMCPMC3986176.
54. Nijland JG, Shin HY, de Jong RM, de Waal PP, Klaassen P, Driessen AJ. Engineering of an endogenous hexose transporter into a specific D-xylose transporter facilitates glucose-xylose co-consumption in Saccharomyces cerevisiae. Biotechnol Biofuels. 2014;7(1):168. doi: 10.1186/s13068-014-0168-9. PubMed PMID: 25505932; PubMed Central PMCID: PMCPMC4263072.

55. Shin HY, Nijland JG, de Waal PP, de Jong RM, Klaassen P, Driessen AJ. An engineered cryptic Hxt11 sugar transporter facilitates glucose-xylose co-consumption in Saccharomyces cerevisiae. Biotechnol Biofuels. 2015;8:176. doi: 10.1186/s13068-015-0360-6. PubMed PMID: 26535057; PubMed Central PMCID: PMCPMC4630928.
56. Roy A, Dement AD, Cho KH, Kim JH. Assessing glucose uptake through the yeast hexose transporter 1 (Hxt1). PLoS One. 2015;10(3):e0121985. doi: 10.1371/journal.pone.0121985. PubMed PMID: 25816250; PubMed Central PMCID: PMC4376911.
57. Nijland JG, Li X, Shin HY, de Waal PP, Driessen AJM. Efficient, D-glucose insensitive, growth on D-xylose by an evolutionary engineered Saccharomyces cerevisiae strain. FEMS Yeast Res. 2019;19(8). doi: 10.1093/femsyr/foz083. PubMed PMID: 31782779.
58. Bermejo C, Haerizadeh F, Takanaga H, Chermak D, Frommer WB. Dynamic analysis of cytosolic glucose and ATP levels in yeast using optical sensors. Biochem J. 2010;432(2):399-406. doi: 10.1042/BJ20100946. PubMed PMID: 20854260; PubMed Central PMCID: PMC2992555.
59. Lang MJ, Martinez-Marquez JY, Prosser DC, Ganser LR, Buelto D, Wendland B, et al. Glucose starvation inhibits autophagy via vacuolar hydrolysis and induces plasma membrane internalization by down-regulating recycling. J Biol Chem. 2014;289(24):16736-47. doi: 10.1074/jbc.M113.525782. PubMed PMID: 24753258; PubMed Central PMCID: PMC4059118.
60. Müller M, Schmidt O, Angelova M, Faserl K, Weys S, Kremser L, et al. The coordinated action of the MVB pathway and autophagy ensures cell survival during starvation. eLife. 2015;4:e07736. doi: 10.7554/eLife.07736. PubMed PMID: 25902403; PubMed Central PMCID: PMCPMC4424281.
61. Ivashov V, Zimmer J, Schwabl S, Kahlhofer J, Weys S, Gstir R, et al. Complementary alpha-arrestin-ubiquitin ligase complexes control nutrient transporter endocytosis in response to amino acids. eLife. 2020;9. doi: 10.7554/eLife.58246. PubMed PMID: 32744498.
62. Volland C, Urban-Grimal D, Geraud G, Haguenauer-Tsapis R. Endocytosis and degradation of the yeast uracil permease under adverse conditions. J Biol Chem. 1994;269(13):9833-41. Epub 1994/04/01. PubMed PMID: 8144575.
63. MacGurn JA, Hsu PC, Smolka MB, Emr SD. TORC1 regulates endocytosis via Npr1-mediated phosphoinhibition of a ubiquitin ligase adaptor. Cell. 2011;147(5):1104-17. Epub 2011/11/29. doi: 10.1016/j.cell.2011.09.054. PubMed PMID: 22118465.
64. Nikko E, Pelham HR. Arrestin-mediated endocytosis of yeast plasma membrane transporters. Traffic. 2009;10(12):1856-67. Epub 2009/11/17. doi: 10.1111/j.1600-0854.2009.00990.x. PubMed PMID: 19912579.
65. Megarioti AH, Primo C, Kapetanakis GC, Athanasopoulos A, Sophianopoulou V, Andre B, et al. The Bul1/2 Alpha-Arrestins Promote Ubiquitylation and Endocytosis of the Can1 Permease upon Cycloheximide-Induced TORC1-Hyperactivation. Int J Mol Sci. 2021;22(19). doi: 10.3390/ijms221910208. PubMed PMID: 34638549; PubMed Central PMCID: PMCPMC8508209.
66. Crapeau M, Merhi A, Andre B. Stress Conditions Promote Yeast Gap1 Permease Ubiquitylation and Down-regulation via the Arrestin-like Bul and Aly Proteins. J Biol Chem. 2014;289(32):22103-16. doi: 10.1074/jbc.M114.582320. PubMed PMID: 24942738; PubMed Central PMCID: PMC4139224.
67. Zhao Y, Macgurn JA, Liu M, Emr S. The ART-Rsp5 ubiquitin ligase network comprises a plasma membrane quality control system that protects yeast cells from proteotoxic stress. eLife. 2013;2:e00459. doi: 10.7554/eLife.00459. PubMed PMID: 23599894; PubMed Central PMCID: PMC3628405.
68. Merhi A, André B. Internal amino acids promote Gap1 permease ubiquitylation via TORC1/Npr1/14-3-3-dependent control of the Bul arrestin-like adaptors. Mol Cell Biol. 2012;32(22):4510-22. Epub 2012/09/12. doi: 10.1128/mcb.00463-12. PubMed PMID: 22966204; PubMed Central PMCID: PMC3486192.
69. Lee S, Ho HC, Tumolo JM, Hsu PC, MacGurn JA. Methionine triggers Ppz-mediated dephosphorylation of Art1 to promote cargo-specific endocytosis. J Cell Biol. 2019;218(3):977-92. doi: 10.1083/jcb.201712144. PubMed PMID: 30610170; PubMed Central PMCID: PMCPMC6400557.
70. Lin CH, MacGurn JA, Chu T, Stefan CJ, Emr SD. Arrestin-related ubiquitin-ligase adaptors regulate endocytosis and protein turnover at the cell surface. Cell. 2008;135(4):714-25. Epub 2008/11/04. doi: 10.1016/j.cell.2008.09.025. PubMed PMID: 18976803.
71. MacDonald C, Shields SB, Williams CA, Winistorfer S, Piper RC. A Cycle of Ubiquitination Regulates Adaptor Function of the Nedd4-Family Ubiquitin Ligase Rsp5. Curr Biol. 2020;30(3):465-79 e5. Epub 2020/01/21. doi: 10.1016/j.cub.2019.11.086. PubMed PMID: 31956026; PubMed Central PMCID: PMCPMC7197006.

72. Wu N, Zheng B, Shaywitz A, Dagon Y, Tower C, Bellinger G, et al. AMPK-dependent degradation of TXNIP upon energy stress leads to enhanced glucose uptake via GLUT1. Mol Cell. 2013;49(6):1167-75. doi: 10.1016/j.molcel.2013.01.035. PubMed PMID: 23453806; PubMed Central PMCID: PMC3615143.
73. Tu J, Carlson M. The GLC7 type 1 protein phosphatase is required for glucose repression in Saccharomyces cerevisiae. Mol Cell Biol. 1994;14(10):6789-96. Epub 1994/10/01. doi: 10.1128/mcb.14.10.6789-6796.1994. PubMed PMID: 7935396; PubMed Central PMCID: PMCPMC359209.
74. Castermans D, Somers I, Kriel J, Louwet W, Wera S, Versele M, et al. Glucose-induced posttranslational activation of protein phosphatases PP2A and PP1 in yeast. Cell Res. 2012;22(6):1058-77. doi: 10.1038/cr.2012.20. PubMed PMID: 22290422; PubMed Central PMCID: PMCPMC3367521.
75. Randez-Gil F, Prieto JA, Sanz P. The expression of a specific 2-deoxyglucose-6P phosphatase prevents catabolite repression mediated by 2-deoxyglucose in yeast. Current genetics. 1995;28(2):101-7. Epub 1995/07/01. PubMed PMID: 8590459.
76. Momcilovic M, Carlson M. Alterations at dispersed sites cause phosphorylation and activation of SNF1 protein kinase during growth on high glucose. J Biol Chem. 2011;286(26):23544-51. Epub 2011/05/13. doi: 10.1074/jbc.M111.244111. PubMed PMID: 21561858.
77. Mueckler M, Thorens B. The SLC2 (GLUT) family of membrane transporters. Molecular aspects of medicine. 2013;34(2-3):121-38. doi: 10.1016/j.mam.2012.07.001. PubMed PMID: 23506862; PubMed Central PMCID: PMCPMC4104978.
78. Bisson LF, Fraenkel DG. Involvement of kinases in glucose and fructose uptake by Saccharomyces cerevisiae. Proc Natl Acad Sci U S A. 1983;80(6):1730-4. Epub 1983/03/01. doi: 10.1073/pnas.80.6.1730. PubMed PMID: 6300872; PubMed Central PMCID: PMCPMC393677.
79. Lagunas R. Sugar transport in Saccharomyces cerevisiae. FEMS Microbiol Rev. 1993;10(3-4):229-42. Epub 1993/04/01. doi: 10.1016/0378-1097(93)90598-v. PubMed PMID: 8318258.
80. Santangelo GM. Glucose signaling in Saccharomyces cerevisiae. Microbiol Mol Biol Rev. 2006;70(1):253-82. doi: 10.1128/MMBR.70.1.253-282.2006. PubMed PMID: 16524925; PubMed Central PMCID: PMCPMC1393250.
81. Vega M, Riera A, Fernandez-Cid A, Herrero P, Moreno F. Hexokinase 2 Is an Intracellular Glucose Sensor of Yeast Cells That Maintains the Structure and Activity of Mig1 Protein Repressor Complex. J Biol Chem. 2016;291(14):7267-85. doi: 10.1074/jbc.M115.711408. PubMed PMID: 26865637; PubMed Central PMCID: PMCPMC4817161.
82. Moreno F, Herrero P. The hexokinase 2-dependent glucose signal transduction pathway of Saccharomyces cerevisiae. FEMS Microbiol Rev. 2002;26(1):83-90. doi: 10.1111/j.1574-6976.2002.tb00600.x. PubMed PMID: 12007644.
83. Ma H, Bloom LM, Walsh CT, Botstein D. The residual enzymatic phosphorylation activity of hexokinase II mutants is correlated with glucose repression in Saccharomyces cerevisiae. Mol Cell Biol. 1989;9(12):5643-9. doi: 10.1128/mcb.9.12.5643-5649.1989. PubMed PMID: 2685572; PubMed Central PMCID: PMCPMC363735.
84. Hovsepian J, Albanese V, Becuwe M, Ivashov V, Teis D, Leon S. The yeast arrestin-related protein Bul1 is a novel actor of glucose-induced endocytosis. Mol Biol Cell. 2018;29(9):1012-20. doi: 10.1091/mbc.E17-07-0466. PubMed PMID: 29514933; PubMed Central PMCID: PMCPMC5921569.
85. Jayakody LN, Kadowaki M, Tsuge K, Horie K, Suzuki A, Hayashi N, et al. SUMO expression shortens the lag phase of Saccharomyces cerevisiae yeast growth caused by complex interactive effects of major mixed fermentation inhibitors found in hot-compressed water-treated lignocellulosic hydrolysate. Appl Microbiol Biotechnol. 2015;99(1):501-15. doi: 10.1007/s00253-014-6174-9. PubMed PMID: 25359478.
86. Brachmann CB, Davies A, Cost GJ, Caputo E, Li J, Hieter P, et al. Designer deletion strains derived from Saccharomyces cerevisiae S288C: a useful set of strains and plasmids for PCR-mediated gene disruption and other applications. Yeast. 1998;14(2):115-32. Epub 1998/03/04. doi: 10.1002/(SICI)1097-0061(19980130)14:2<115::AID-YEA204>3.0.CO;2-2. PubMed PMID: 9483801.
87. Hovsepian J, Defenouillere Q, Albanese V, Vachova L, Garcia C, Palkova Z, et al. Multilevel regulation of an alpha-arrestin by glucose depletion controls hexose transporter endocytosis. J Cell Biol. 2017;216(6):1811-31. Epub 2017/05/05. doi: 10.1083/jcb.201610094. PubMed PMID: 28468835; PubMed Central PMCID: PMCPMC5461024.
88. Huh WK, Falvo JV, Gerke LC, Carroll AS, Howson RW, Weissman JS, et al. Global analysis of protein localization in budding yeast. Nature. 2003;425(6959):686-91. PubMed PMID: 14562095.
89. Dohmen RJ, Stappen R, McGrath JP, Forrova H, Kolarov J, Goffeau A, et al. An essential yeast gene encoding a homolog of ubiquitin-activating enzyme. J Biol Chem. 1995;270(30):18099-109. doi: 10.1074/jbc.270.30.18099. PubMed PMID: 7629121.

867 # Acknowledgments

868

869 We thank Agathe Verraes for technical assistance, Olivier Vincent (CSIC, Madrid, Spain) and Michel Becuwe
870 (Harvard University, Cambridge, MA, USA) for sharing reagents and Alexandre Soulard (Université Claude
871 Bernard Lyon 1, Lyon, France) for helpful discussions and critical reading of the manuscript. We also
872 acknowledge the IJM ImagoSeine facility, member of IBiSA and the France-BioImaging infrastructure
873 (https://anr.fr/ProjetIA-10-INBS-0004; ANR-10-INBS-04). This work was supported by grants from the
874 Fondation ARC pour la recherche sur le cancer (https://www.fondation-arc.org, ARCPJA32020060002096 to
875 SL), Université de Paris IDEx (https://u-paris.fr; ANR-18-IDEX-0001, "Emergence en Recherche"
876 RS30J20IDXA1_EMERLEON) and individual fellowships from the Ligue contre le cancer (https://www.ligue-
877 cancer.net; TAZK20115 to CL), the Fondation pour la Recherche Médicale (https://www.frm.org;
878 SPF20150934065 to QD) and the French Ministry for Research and Education (https://www.enseignementsup-
879 recherche.gouv.fr; to AB). The funders had no role in study design, data collection and analysis, decision to
880 publish, or preparation of the manuscript.
881 **Competing interests:** The authors have declared that no competing interests exist.

Supplementary materials

Table S1: Yeast strains used in this study

Name	Genotype & Description	Origin & Reference
ySL0066: **BY4741 (WT)**	*MAT a; ura3Δ0, his3Δ1, leu2Δ0, met15Δ0*	[86]
ySL0534: ***rod1Δ***	*MAT a; ura3Δ0, his3Δ1, leu2Δ0, met15Δ0 rod1Δ::KANMX*	Léon lab
ySL0541: ***reg1Δ***	*MAT a; ura3Δ0, his3Δ1, leu2Δ0, met15Δ0 reg1Δ::HIS3MX*	[28]
ySL0567: ***snf1Δ***	*Mat alpha, ura3Δ0, his3Δ1, leu2Δ0, lys2Δ0, snf1Δ::kanMX4*	Léon lab
ySL0854: ***cnb1Δ***	*MAT a,ura3Δ0, his3Δ1, leu2Δ0, met15Δ0 cnb1Δ::KANMX*	Léon lab
ySL1027: **Hxt3-GFP**	*MAT a; ura3Δ0, his3Δ1, leu2Δ0, met15Δ0 HXT3::GFP-HIS3MX*	[87]
ySL1140: **Hxt2-GFP**	*MAT a;ura3Δ0, his3Δ1, leu2Δ0, met15Δ0 HXT2::GFP-HIS3MX*	[87]
ySL1186: **Hxt1-GFP**	*MAT a; ura3Δ0, his3Δ1, leu2Δ0, met15Δ0 HXT1::GFP-HIS3MX*	[87]
ySL1690: ***hxk2Δ***	*MAT a; ura3Δ0, his3Δ1, leu2Δ0, met15Δ0 hxk2Δ::KANMX*	Léon lab
ySL1852 : **Hxt4-GFP**	*MAT a; ura3Δ0, his3Δ1, leu2Δ0, met15Δ0 HXT4::GFP-HIS3MX*	[87]
ySL1961: ***slt2Δ***	*MAT a; ura3Δ0, his3Δ1, leu2Δ0, met15Δ0 slt2Δ::KANMX*	Euroscarf
ySL2092: **Vht1-GFP**	*MAT a; ura3Δ0, his3Δ1, leu2Δ0, met15Δ0 VHT1::GFP-HIS3MX*	[88]
ySL2110: **Pdr12-GFP**	*MAT a; ura3Δ0, his3Δ1, leu2Δ0, met15Δ0 PDR12::GFP-HIS3MX*	[88]
ySL2119: **Bap2-GFP**	*MAT a; ura3Δ0, his3Δ1, leu2Δ0, met15Δ0 BAP2::GFP-HIS3MX*	[88]
ySL2123: **Fps1-GFP**	*MAT a; ura3Δ0, his3Δ1, leu2Δ0, met15Δ0 FPS1::GFP-HIS3MX*	[88]
ySL2132: **Mid2-GFP**	*MAT a; ura3Δ0, his3Δ1, leu2Δ0, met15Δ0 MID2::GFP-HIS3MX*	[88]
ySL2142: **Qdr3-GFP**	*MAT a; ura3Δ0, his3Δ1, leu2Δ0, met15Δ0 QDR3::GFP-HIS3MX*	[88]
ySL2169: **Slg1-GFP**	*MAT a; ura3Δ0, his3Δ1, leu2Δ0, met15Δ0 SLG1::GFP-HIS3MX*	[88]
ySL2175: **Ste2-GFP**	*MAT a; ura3Δ0, his3Δ1, leu2Δ0, met15Δ0 STE2::GFP-HIS3MX*	[88]
ySL2204: ***hac1Δ***	*MAT a; ura3Δ0, his3Δ1, leu2Δ0, met15Δ0 hac1Δ::KANMX*	Euroscarf
ySL2216: **Itr1-GFP *snf1Δ***	*MAT a; ura3Δ0, his3Δ1, leu2Δ0, met15Δ0 snf1Δ::HPHNT1 Itr1::GFP-HIS3MX*	This study
ySL2219: **Tat1-GFP**	*MAT a; ura3Δ0, his3Δ1, leu2Δ0, met15Δ0 TAT1::GFP-HIS3MX*	[88]

ySL2221: **Can1-GFP**	*MAT a; ura3Δ0, his3Δ1, leu2Δ0, met15Δ0 CAN1::GFP-HIS3MX*	[88]
ySL2222: **Lyp1-GFP**	*MAT a; ura3Δ0, his3Δ1, leu2Δ0, met15Δ0 LYP1::GFP-HIS3MX*	[88]
ySL2223: **Fui1-GFP**	*MAT a; ura3Δ0, his3Δ1, leu2Δ0, met15Δ0 FUI1::GFP-HIS3MX*	[88]
ySL2224: **Itr1-GFP**	*MAT a; ura3Δ0, his3Δ1, leu2Δ0, met15Δ0 ITR1::GFP-HIS3MX*	[88]
ySL2237: **Pdr12-GFP *snf1Δ***	*MAT a; ura3Δ0, his3Δ1, leu2Δ0, met15Δ0 PDR12::GFP-HIS3MX snf1Δ::NATNT2*	This study
ySL2288: **Ina1-GFP**	*MAT a; ura3Δ0, his3Δ1, leu2Δ0, met15Δ0 INA1::GFP-HIS3MX*	[88]
ySL2315: ***hog1Δ***	*MAT a; ura3Δ0, his3Δ1, leu2Δ0, met15Δ0 hog1Δ::KANMX*	Euroscarf
ySL2325: **Ina1-GFP *npi1***	*MAT a; ura3Δ0, his3Δ1, leu2Δ0, met15Δ0 INA1::GFP-HIS3MX pRSP5::KANMX*	This study
ySL2395: **Ina1-GFP *snf1Δ***	*MAT a; ura3Δ0, his3Δ1, leu2Δ0, met15Δ0 snf1Δ::HIS3MX INA1::GFP-HPHNT1*	This study
ySL2406: **Ina1-GFP *rod1Δ***	*MAT a; ura3Δ0, his3Δ1, leu2Δ0, met15Δ0 INA1::GFP-HPHNT1 rod1Δ::KANMX*	This study
ySL2412: **Ina1-GFP *rvs167Δ***	*MAT a; ura3Δ0, his3Δ1, leu2Δ0, met15Δ0 rvs167ΔKANMX4 INA1::GFP-HPHNT1*	This study
ySL2434: **Ina1-Δ5-GFP**	*MAT a; ura3Δ0, his3Δ1, leu2Δ0, met15Δ0 Ina1-Δ5::GFP-KANMX*	This study
ySL2443: **Pil1-GFP**	*MAT a; ura3Δ0, his3Δ1, leu2Δ0, met15Δ0 PIL1::GFP-HIS3MX*	[88]
ySL2444: **Sur7-GFP**	*MAT a; ura3Δ0, his3Δ1, leu2Δ0, met15Δ0 SUR7::GFP-HIS3MX*	[88]
ySL2445: **Lsp1-GFP**	*MAT a; ura3Δ0, his3Δ1, leu2Δ0, met15Δ0 LSP1::GFP-HIS3MX*	[88]
ySL2446: **Seg1-GFP**	*MAT a; ura3Δ0, his3Δ1, leu2Δ0, met15Δ0 SEG1::GFP-HIS3MX*	[88]
ySL2451: **Lyp1-GFP *rod1Δ***	*MAT a; ura3Δ0, his3Δ1, leu2Δ0, met15Δ0 LYP1::GFP-HIS3MX rod1Δ::KANMX*	This study
ySL2452: **Qdr3-GFP *rod1Δ***	*MAT a; ura3Δ0, his3Δ1, leu2Δ0, met15Δ0 QDR3::GFP-HIS3MX rod1Δ::KANMX*	This study
ySL2545: **Tat1-GFP *rod1Δ***	*MAT a; ura3Δ0, his3Δ1, leu2Δ0, met15Δ0 TAT1::GFP-HIS3MX rod1Δ::KANMX*	This study
ySL2546: **Fui1-GFP *rod1Δ***	*MAT a; ura3Δ0, his3Δ1, leu2Δ0, met15Δ0 FUI1::GFP-HIS3MX rod1Δ::KANMX*	This study
ySL2548: ***rvs167Δ***	*MAT a; ura3Δ0, his3Δ1, leu2Δ0, met15Δ0 rvs167Δ::KANMX*	Euroscarf

ySL2580: **Vht1-GFP *rod1Δ***	*MAT a; ura3Δ0, his3Δ1, leu2Δ0, met15Δ0 VHT1::GFP-HIS3MX rod1Δ::URA3*	This study
ySL2591: **Ste2-GFP *rod1Δ***	*MAT a; ura3Δ0, his3Δ1, leu2Δ0, met15Δ0 STE2::GFP-HIS3MX rod1Δ::URA3*	This study
ySL2592: **Can1-GFP *rod1Δ***	*MAT a; ura3Δ0, his3Δ1, leu2Δ0, met15Δ0 CAN1::GFP-HIS3MX rod1Δ::URA3*	This study
ySL2623: **Wsc3-GFP**	*MAT a; ura3Δ0, his3Δ1, leu2Δ0, met15Δ0 WSC3::GFP-HIS3MX*	[88]
ySL2628: **Wsc2-GFP**	*MAT a; ura3Δ0, his3Δ1, leu2Δ0, met15Δ0 WSC2::GFP-HIS3MX*	[88]
ySL2671: **Ina1-GFP *hxk2Δ***	*MAT a; ura3Δ0, his3Δ1, leu2Δ0, met15Δ0 ; INA1::GFP-HIS3MX hxk2Δ::KANMX*	This study
ySL2724: **Hxt1-GFP *rod1Δ***	*MAT a; ura3Δ0, his3Δ1, leu2Δ0, met15Δ0 HXT1::GFP-HIS3MX rod1Δ::HPHNT1*	This study
ySL2725: **Hxt3-GFP *rod1Δ***	*MAT a; ura3Δ0, his3Δ1, leu2Δ0, met15Δ0 HXT3::GFP-HIS3MX rod1Δ::HPHNT1*	This study
ySL2726: **Itr1-GFP *rod1Δ***	*MAT a; ura3Δ0, his3Δ1, leu2Δ0, met15Δ0 ITR1::GFP-HIS3MX rod1Δ::HPHNT1*	This study
ySL2727: **Pdr12-GFP *rod1Δ***	*MAT a; ura3Δ0, his3Δ1, leu2Δ0, met15Δ0 PDR12::GFP-HIS3MX rod1Δ::HPHNT1*	This study
ySL2728: **Lyp1-GFP *rod1Δ rog3Δ***	*MAT a; ura3Δ0, his3Δ1, leu2Δ0, met15Δ0 LYP1::GFP-HIS3MX rod1Δ::KANMX; rog3Δ::NATNT2*	This study
ySL2739: **Vph1-mCherry**	*MAT a; ura3Δ0, his3Δ1, leu2Δ0, met15Δ0 ; Vph1-mCherry::NATNT2*	This study
ySL2746: ***rod1Δ hxt6Δ***	*MAT a; ura3Δ0, his3Δ1, leu2Δ0, met15Δ0 rod1Δ::KANMX hxt6Δ::NATNT2*	This study
ySL2880: **Ina1-GFP Pil1-mCherry**	*MAT a; ura3Δ0, his3Δ1, leu2Δ0, met15Δ0 INA1::GFP-HIS3MX PIL1::mCherry-NATNT2*	This study
ySL3003: ***rod1Δ* Hxt3-GFP**	*MAT a; ura3Δ0, his3Δ1, leu2Δ0, met15Δ0 rod1Δ::KANMX Hxt3::GFP-HPHNT1*	This study
ySL3026: ***hxt3Δ***	*MAT a; ura3Δ0, his3Δ1, leu2Δ0, met15Δ0 hxt3Δ::KANMX*	Euroscarf
ySL3027: ***rod1Δhxt3Δ***	*MAT a; ura3Δ0, his3Δ1, leu2Δ0, met15Δ0 hxt3Δ::KANMX rod1Δ::HPHNT1*	This study
ySL3028: ***hxt1Δ***	*MAT a; ura3Δ0, his3Δ1, leu2Δ0, met15Δ0 hxt1Δ::KANMX*	Euroscarf
ySL3029: ***rod1Δhxt1Δ***	*MAT a; ura3Δ0, his3Δ1, leu2Δ0, met15Δ0 hxt1Δ::KANMX rod1Δ::HPHNT1*	This study
ySL3084: ***hxt1Δhxt3Δ***	*MAT a; ura3Δ0, his3Δ1, leu2Δ0, met15Δ0 hxt1Δ::KANMX hxt3Δ::HPHNT1*	This study

ySL3099: ***rod1Δ dog1Δ dog2Δ***	*MAT a; ura3Δ0, his3Δ1, leu2Δ0, met15Δ0 rod1Δ::KANMX dog1Δdog2Δ::LEU2*	This study
ySL3118 : **Hxt4-GFP *rod1Δ***	*MAT a; ura3Δ0, his3Δ1, leu2Δ0, met15Δ0 HXT4::GFP-HIS3MX rod1Δ::KANMX*	This study
ySL3124: **Hxt2-GFP *rod1Δ***	*MAT a; ura3Δ0, his3Δ1, leu2Δ0, met15Δ0 HXT2::GFP-HIS3MX rod1Δ::HPHNT1*	This study

884

885 **Table S2: Plasmids used in this study**

Name	Description	Origin & Reference
pSL093	pRS416-derived (CEN, *URA3*) p_{ROD1}*:ROD1*-GFP	[35]
pSL094	pRS415-derived (CEN, *LEU2*) p_{ROD1}*:ROD1*-3HA	[28]
pSL205	p_{CUP1}:6xHis-Ub (2µ, *LEU2*) (pJD421)	[89]
pSL237	pRS316-derived (CEN, *URA3*) p_{Rod1}:Rod1-3Flag	Olivier Vincent
pSL409	*Yep358-based (2µ, URA3)* p_{DOG1}*(1000bp):LacZ*	[20]
pSL410	*Yep358-based (2µ, URA3)* p_{DOG2}*(1000bp):LacZ*	[20]
pSL412	pRS426-derived (2µ, *URA3*) p_{GPD}*:DOG2*	[20]
pSL436	pRS426-derived (2µ, *URA3*) p_{GPD}*:DOG2(DD>AA)*	[20]
pSL559	pRS313-derived (CEN, *HIS3*) p_{ROD1}*:ROD1*-Flag	This study
pSL560	pRS313-derived (CEN, *HIS3*) p_{ROD1}*:ROD1-PYm*-Flag	This study
pSL561	pRS313-derived (CEN, *HIS3*) p_{ROD1}*:ROD1-S12A*-Flag	This study
pSL563	pRS313-derived (CEN, *HIS3*) p_{ROD1}*:ROD1-KR*-Flag	This study
pSL589	pUG35-derived (ARS/CEN, *URA3*) *pHXT3:HXT3*-GFP	This study
pSL590	pDRf1GW-ura3-derived (2µ, *URA3*) FLII12Pglu-700µδ6 Glucose FRET sensor, Addgene #28002	Wolf Frommer [58]
pSL591	pUG35-derived (ARS/CEN, *URA3*) *pHXT3:HXT3(N370A)*-GFP	This study
pSL599	pRS426-derived (2µ, *URA3*) p_{HXT1}*:HXT1*	This study
pSL602	pRS426-derived (2µ, *URA3*) p_{HXT3}*:HXT3*	This study

pSL608	pDRF1-GW-derived (2µ, *URA3*), yAT1.03 ATP FRET sensor, Addgene #132781	Bas Teusink [48]
pSL609	pDRF1-GW-derived (2µ, *URA3*), yAT1.03 ATP FRET sensor, mutated R122K,R126K (non-ATP binding), Addgene #132782	Bas Teusink [48]

886

887 **Table S3: Antibodies used this study**

Name	Description	Dilution	Reference/Origin
α GFP	Mouse monoclonal against GFP, clones 7.1/ 13.1	1/5000	11814460001 -Roche
α Flag	Mouse monoclonal antibody against Flag	1/5000	F3165 - Sigma
α pAMPK / pSnf1	Rabbit polyclonal antibody against Thr172-phosphorylated human AMPKα	1/1000	#2535 – Cell Signaling Technology
α polyHis tag	Mouse monoclonal antibody to reveal Snf1 (contains a stretch of 13 His residues), or poly-His-tagged proteins	1/2000	H1029 - Sigma
α Ubiquitin	Mouse monoclonal antibody against ubiquitin	1/1000	P4D1 - Santa Cruz
α Rabbit IgG	Goat secondary antibody against Rabbit IgG (HRP)	1/5000	A6154 - Sigma
α Mouse IgG	Goat secondary antibody against Mouse IgG (HRP)	1/5000	A5278 - Sigma

888

A.

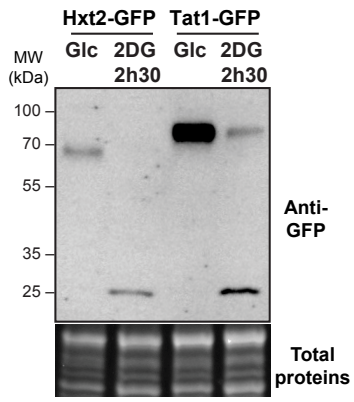

B.

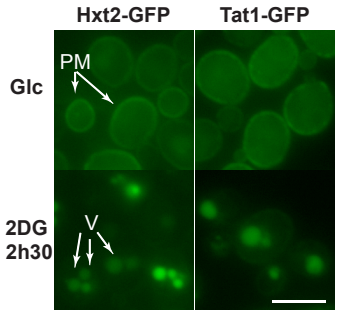

C.

Name	Function	Endocytosis ?	Rod1-depdt?
Hxt1	Glucose transporter (low aff)	Yes	Yes
Hxt3	Glucose transporter (low aff)	Yes	Yes
Hxt2	Glucose transporter (med/high aff)	Yes	Yes
Hxt4	Glucose transporter (med/high aff)	Yes	Yes
Qdr3	Multidrug transporter (MFS type)	Yes	Yes
Pdr12	Multidrug transporter (ABC type)	Yes	Yes
Vht1	Biotin transporter	Yes	No
Fui1	Uridine permease	Yes	Yes
Tat1	Tryptophan permease	Yes	Yes
Lyp1	Lysine permease	Yes	No
Can1	Arginine permease	Yes	No
Itr1	Inositol transporter	Yes	Yes
Bap2	Leucine permease	Yes	NT
Ste2	GPCR (α-factor pheromone)	Yes	No
Ina1	Unknown	Yes	Yes
Slg1/Wsc1	Cell wall stress sensor	No	-
Wsc2	Cell wall stress sensor	No	-
Wsc3	Cell wall stress sensor	No	-
Mid2	Cell wall stress sensor	No	-
Fps1	Aquaglyceroporin	No	-

D.

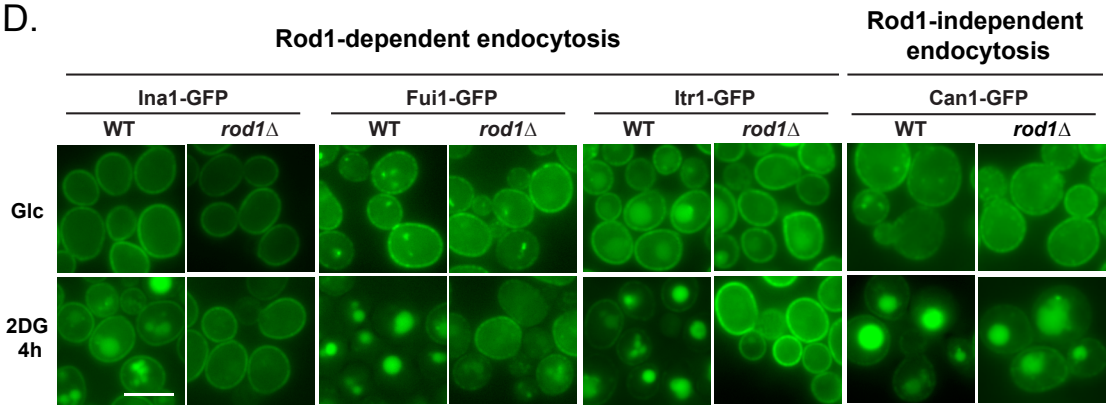

Laussel et al. Fig 1

Figure 1 - 2DG treatment induces the endocytosis of many plasma membrane proteins, that is mostly Rod1-dependent. (**A**) Western blot on total protein extracts from Hxt2-GFP- and Tat1-GFP-expressing cells before and after addition for 2h30, using anti-GFP antibodies. (**B**) Cells expressing Hxt2-GFP and Tat1-GFP cells were grown overnight in a glucose-containing medium (exponential phase) and treated with 2DG for 2h30 and observed by fluorescence microscopy. PM: plasma membrane ; V: vacuole. Scale bar: 5 µm. (**C**) Plasma membrane proteins whose localization was examined by fluorescence microscopy before and after 2h30 2DG. When endocytosed, the same proteins were also observed in a *rod1Δ* context to check for Rod1 dependence (NT, not tested). (**D**) Fluorescence microscopy of WT and *rod1Δ* cells expressing the indicated transporters tagged with GFP before and after 2DG treatment for 4h. Scale bar: 5 µm.

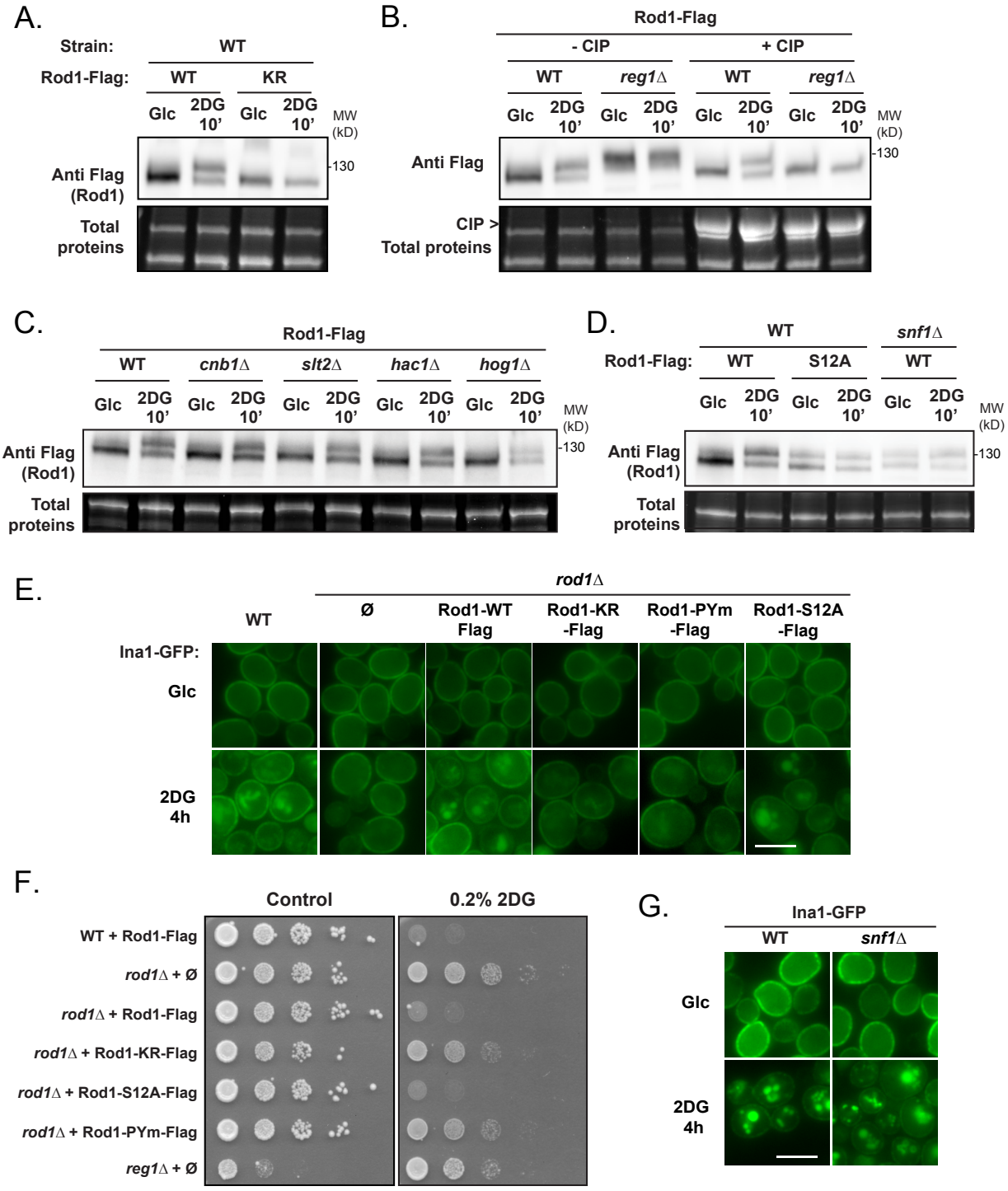

Laussel et al. Fig 2

Figure 2 - Following 2DG treatment, Rod1 is dephosphorylated in a PP1-dependent manner. (A) Total protein extracts of WT cells expressing either Rod1-Flag or Rod1-KR-Flag were prepared before and after 2DG addition for 10', and immunoblotted using an anti-Flag antibody. **(B)** Total protein extracts of WT or *reg1Δ* cells expressing Rod1-Flag were prepared before and after 2DG addition for 10', and immunoblotted using an anti-

905 Flag antibody. Samples were dephosphorylated by CIP where indicated. **(C)** Total protein extracts of WT,
906 *cnb1Δ, slt2Δ*, *hac1Δ,* or *hog1Δ* expressing Rod1-Flag were prepared before and after 2DG addition for 10', and
907 immunoblotted using an anti-Flag antibody. **(D)** Total protein extract of WT or *snf1Δ* cells expressing Rod1-Flag
908 or Rod1-S12A-Flag were prepared before and after 2DG addition for 10' using an anti-Flag antibody. **(E)** WT or
909 *rod1Δ* cells expressing the various *ROD1*-Flag constructs were grown in a glucose-containing medium and
910 observed by fluorescence microscopy before and after 2DG treatment for 4h. Scale bar, 5 µm. **(F)** Serial
911 dilutions of cultures of the indicated strains were spotted on SC medium or SC + 0,2% 2DG medium and grown
912 for 4 days at 30°C. **(G)** WT or *snf1Δ* cells expressing Ina1-GFP were grown in a glucose-containing medium and
913 observed by fluorescence microscopy before and after 2DG treatment for 4h. Scale bar, 5 µm.
914

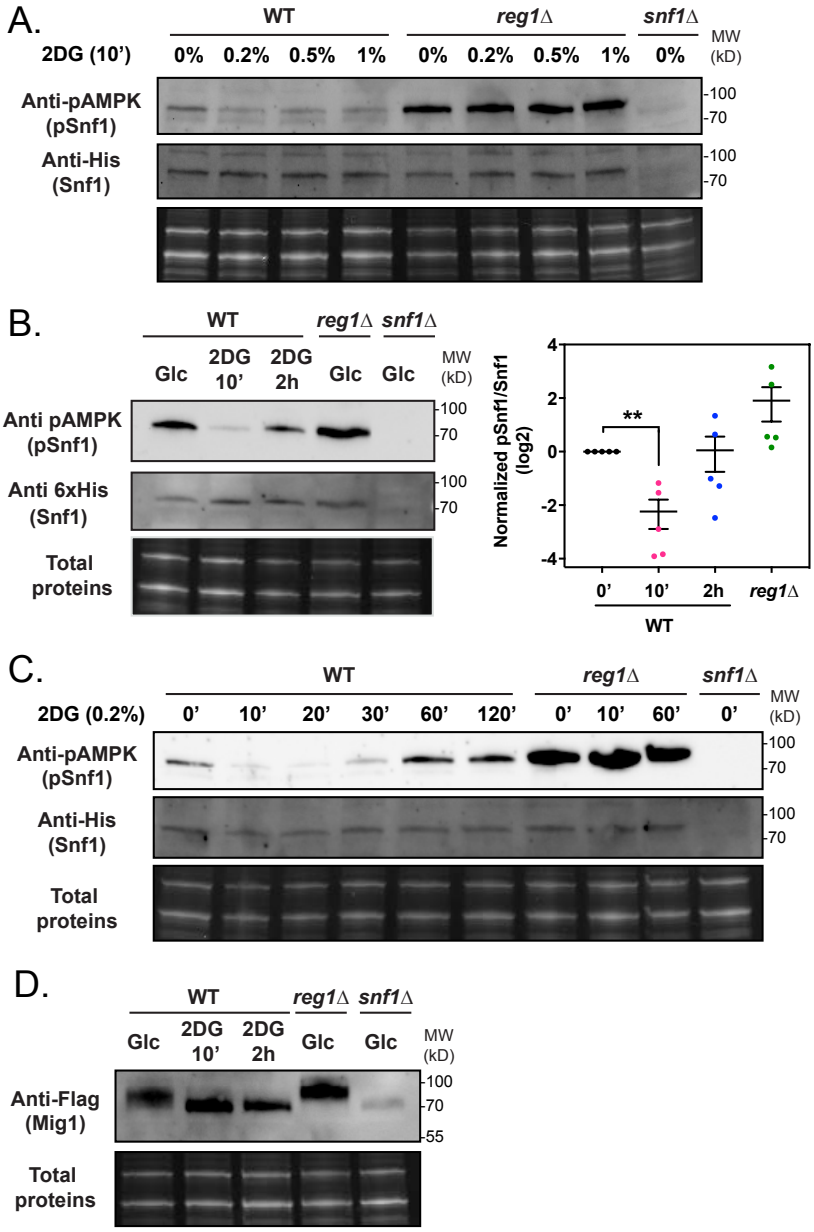

Laussel et al. Fig 3

Figure 3 - 2DG causes a fast and temporary dephosphorylation of Snf1 and its substrates through PP1 activation (A) Total protein extracts of WT, *reg1Δ* and *snf1Δ* cells expressing Mig1-Flag were prepared before and after 2DG addition at the indicated concentrations for 10 min and immunoblotted using anti-phospho-AMPK and anti-polyHistidine antibodies. **(B)** *Left*, Total protein extracts of WT, *reg1Δ* and *snf1Δ* cells were prepared before and after 2DG addition for the indicated time and immunoblotted using anti-phospho-AMPK and anti-polyHistidine antibodies. *Right,* quantification of the signals. **: *p*-value ≤ 0,01 **(C)** Total protein extracts of WT, *reg1Δ* and *snf1Δ* cells were prepared before and after 2DG addition for the indicated time and immunoblotted using anti-phospho-AMPK and anti-polyHistidine antibodies. **(D)** Total protein extracts of WT, *reg1Δ* and *snf1Δ* cells expressing Mig1-Flag were prepared before or after 2DG addition for 10' and 2h and immunoblotted using anti-Flag antibodies.

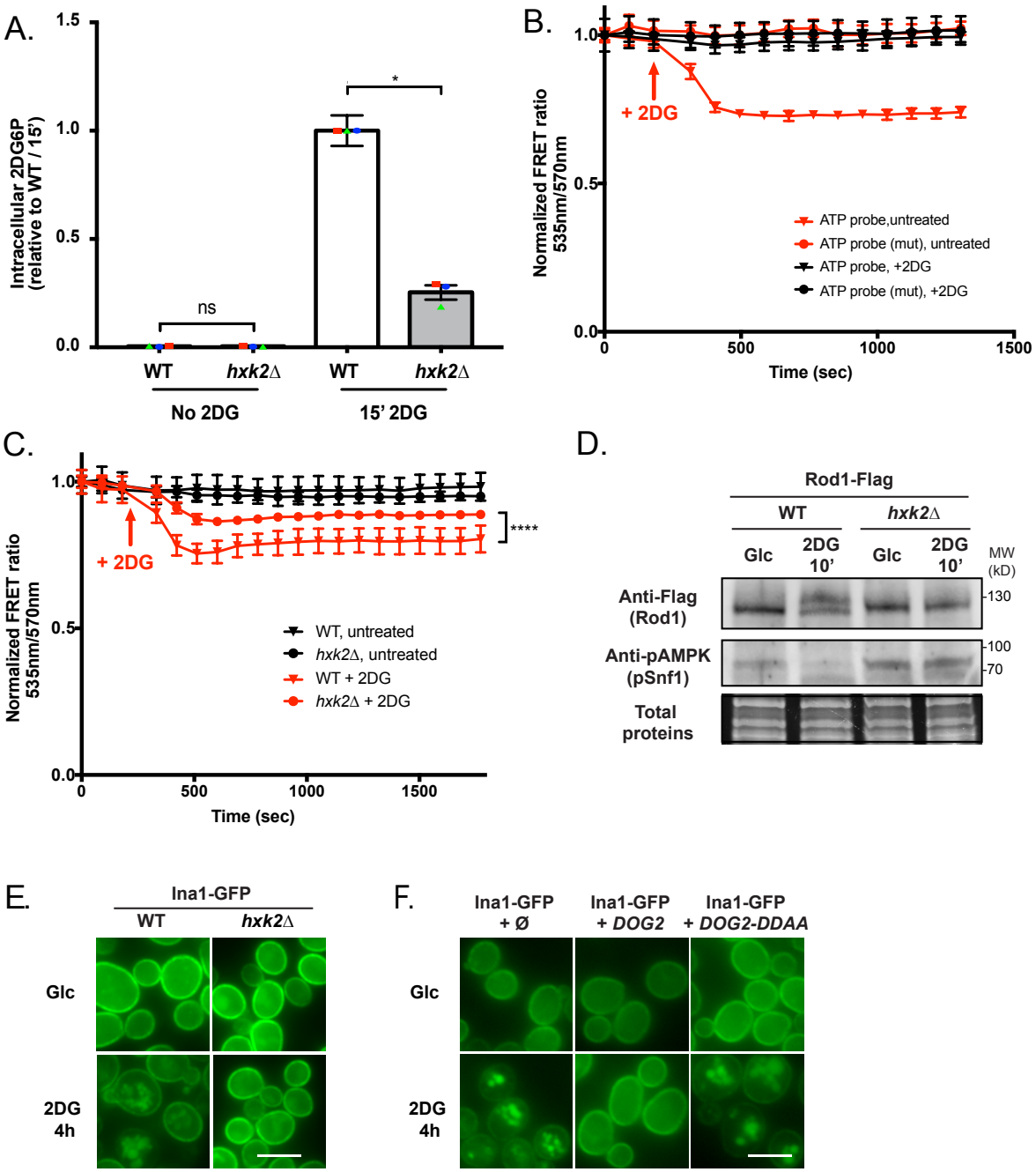

Laussel et al. Fig 4

Figure 4 - Hexokinase 2 (Hxk2) is the main 2DG-phosphorylating enzyme *in vivo* (**A**) Intracellular 2DG6P was assayed enzymatically (see Methods) in WT and *hxk2Δ* cells grown overnight in a glucose-containing medium and treated or not for 15 min with 0.2% 2DG. Values are normalized to the value of the WT / 15 min (n=3 independent experiments ± SD, paired *t*-test) (**B**) 2DG causes a decrease in ATP content as visualized using a FRET ATP biosensor. Cells were grown overnight in a glucose-containing medium and treated with 0.2% 2DG (arrow). The FRET ratio (535/570 nm) was measured over time in a plate reader (see Methods) and is represented as normalized to the t0 value. (*n*=3 independent experiments ± SEM). (**C**) ATP levels were measured as in (B) in WT and *hxk2Δ* cells in response to 2DG. The FRET ratio (535/570 nm) is represented as normalized to the t0 value (n=4 independent experiments ± SEM). A paired *t*-test was used to compare WT +

2DG vs *hxk2Δ* + 2DG (****: p<0.0001). (**D**) Total protein extracts of WT and *hxk2Δ* expressing Rod1-Flag were prepared before and after 10' 2DG treatment and immunoblotted using anti-Flag, anti-phospho-AMPK and anti-polyHistidine antibodies. (**E**) WT or *hxk2Δ* cells expressing Ina1-GFP were grown in a glucose-containing medium and observed by fluorescence microscopy before and after 2DG treatment for 4h. Scale bar, 5 µm. (**F**) WT cells expressing Ina1-GFP and transformed with an empty plasmid, or with plasmids allowing the overexpression of *DOG2* or its catalytic mutant *DOG2-DDAA* were grown in a glucose-containing medium and observed by fluorescence microscopy before and after 2DG treatment for 4h. Scale bar, 5 µm.

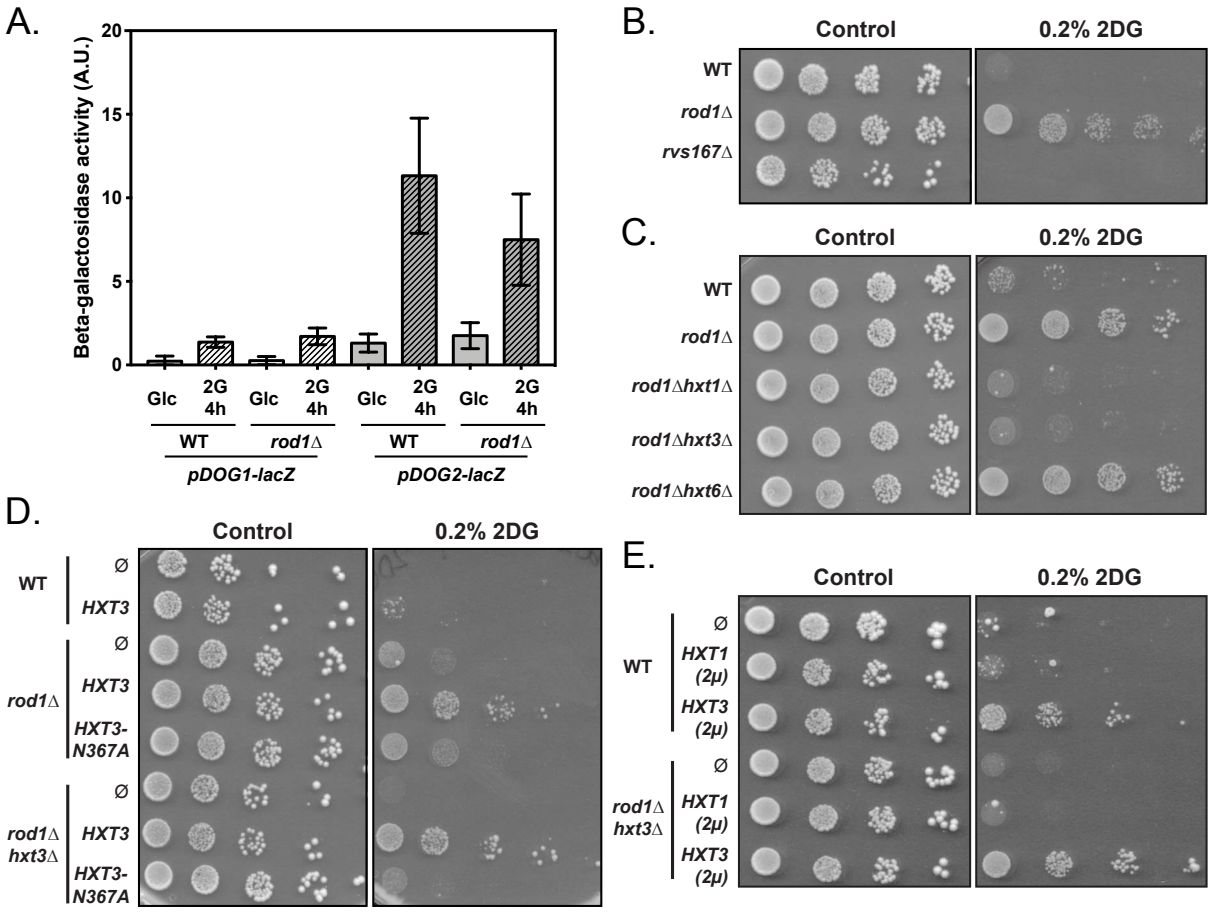

Laussel et al. Fig 5

Figure 5- Low affinity glucose transporters are required for the resistance of the *rod1Δ* mutant to 2DG

(**A**) Beta-galactosidase assays of WT and *rod1Δ* cells expressing *LacZ* under the control of the p*DOG1* or p*DOG2* promoters, before and after 2DG treatments for 4h (+- SEM, n=3 independent experiments, *t*-test). A.U., arbitrary units. (**B-E**) Serial dilutions of cultures of the indicated strains were spotted on SC medium or SC + 0,2% 2DG medium and grown for 3-5 days at 30°C.

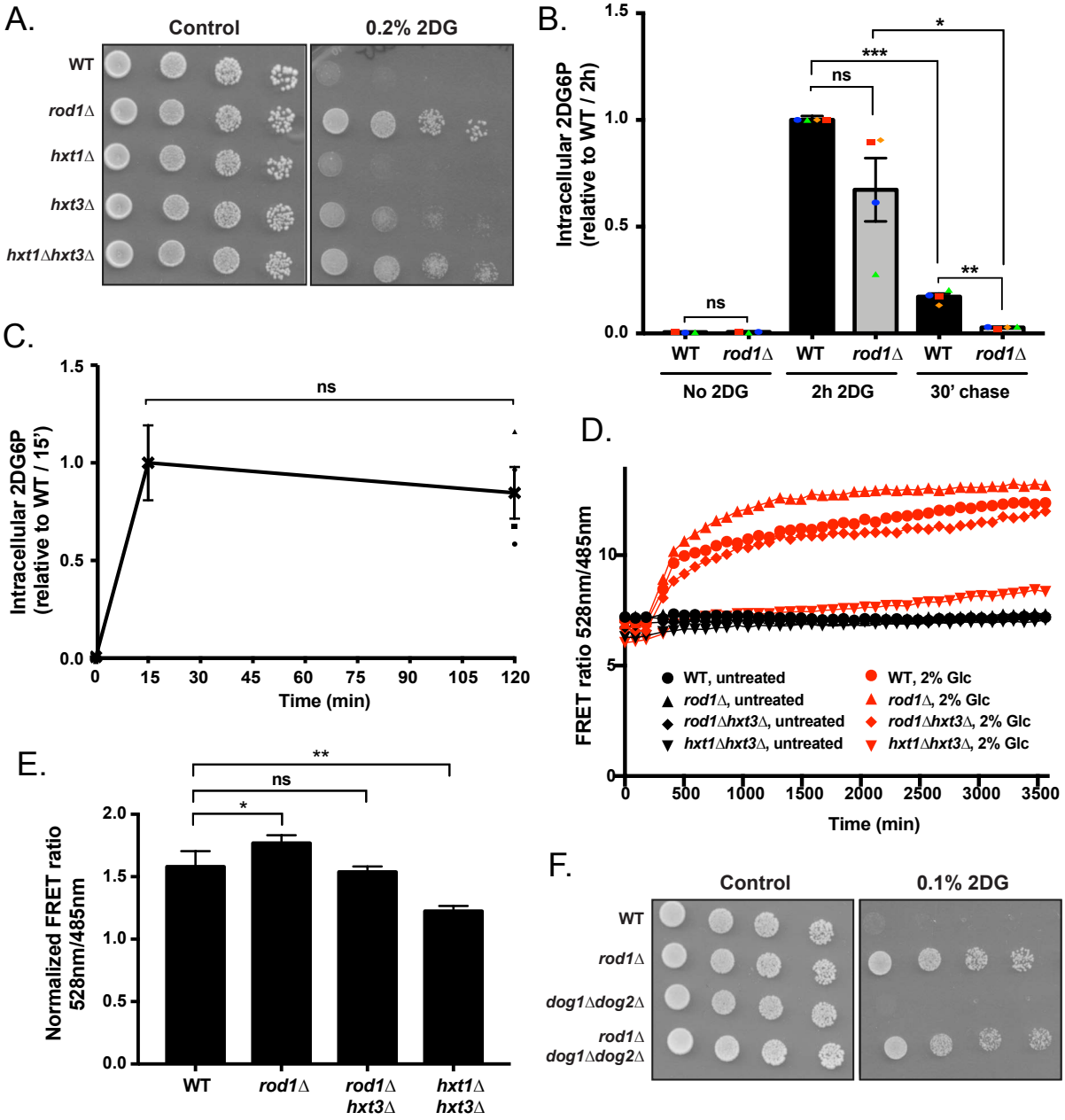

Laussel et al. Fig 6

Figure 6- The maintenance of glucose transporters in the *rod1Δ* mutant promotes 2DG resistance by increasing glucose uptake and limiting 2DG toxicity (**A**) Serial dilutions of cultures of the indicated strains were spotted on SC medium or SC + 0,2% 2DG medium and grown for 3-5 days at 30°C. (**B**) Intracellular 2DG6P was assayed enzymatically in WT and *rod1Δ* cells grown overnight in a glucose-containing medium, treated for 2h with 0.2% 2DG, and then transferred into a 2DG-free glucose-containing medium ("chase"). Values are normalized to the value of the WT / 2h (n=4 independent experiments ± SEM, paired *t*-test). (**C**) 2DG6P content was assayed from WT cells as in (**B**) after 15 min and 2h treatment with 0.2% 2DG. (**D**) Intracellular glucose measurement using a FRET-based glucose biosensor (representative experiment). Cells were grown overnight in glucose medium (exponential phase), treated for 4h with 0.2% 2DG, and transferred in a glucose-free buffer. Fluorescence at 485 and 528 nm was measured every 90 sec in a plate reader before and after glucose addition

964 (2%) (see Methods) and the FRET ratio (485/528 nm) is indicated over time. (**E**) Intracellular glucose was
965 evaluated as in (**D**) at 2000 sec across *n*=5 independent experiments (± SEM, paired *t*-test) and is represented
966 as normalized to the "before glucose" value. (**F**) Serial dilutions of cultures of the indicated strains were spotted
967 on SC medium or SC + 0,1% 2DG medium and grown for 3-5 days at 30°C.
968

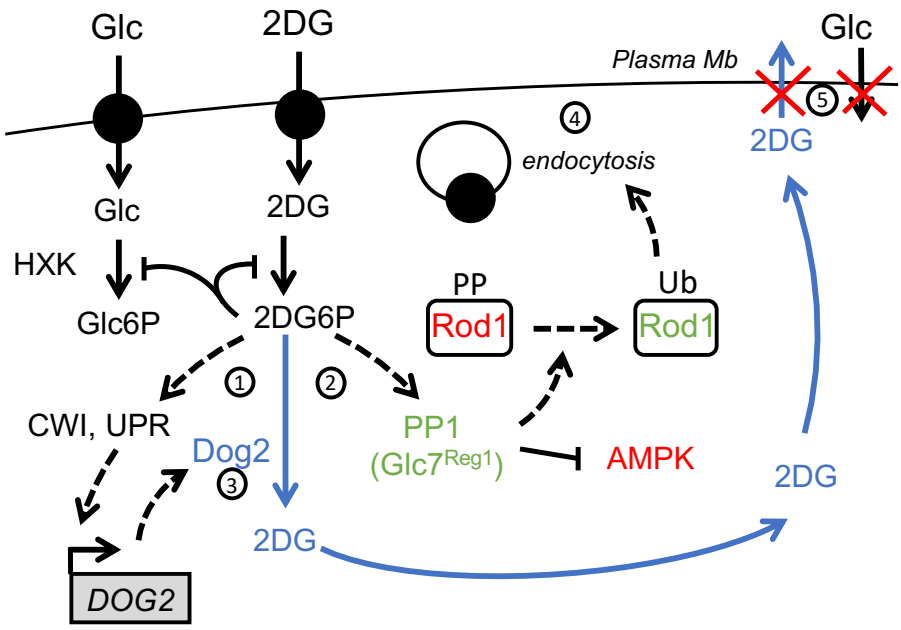

969
970

971 Laussel et al. Fig 7

972

973 **Figure 7 - Hypothetical model for a role of hexose transporters in 2DG detoxification.** Treatment of cells
974 with 2DG triggers the accumulation of intracellular 2DG6P. This activates stress-signaling pathways such as
975 cell-wall integrity signaling (CWI) or the unfolded protein response (UPR), converging onto *DOG2* expression
976 (1) [20]. On the other hand, 2DG6P elicits a fast PP1 activation (2) which causes AMPK inhibition and, either
977 directly or indirectly, Rod1 dephosphorylation. By the time Dog2 is induced and begins to dephosphorylate
978 2DG6P (3), Rod1 has already triggered the endocytosis of many plasma membrane proteins (4), including that
979 of low affinity glucose transporters. This may prevent 2DG exit and detoxification but also affect cell survival
980 by reducing glucose import (5).
981

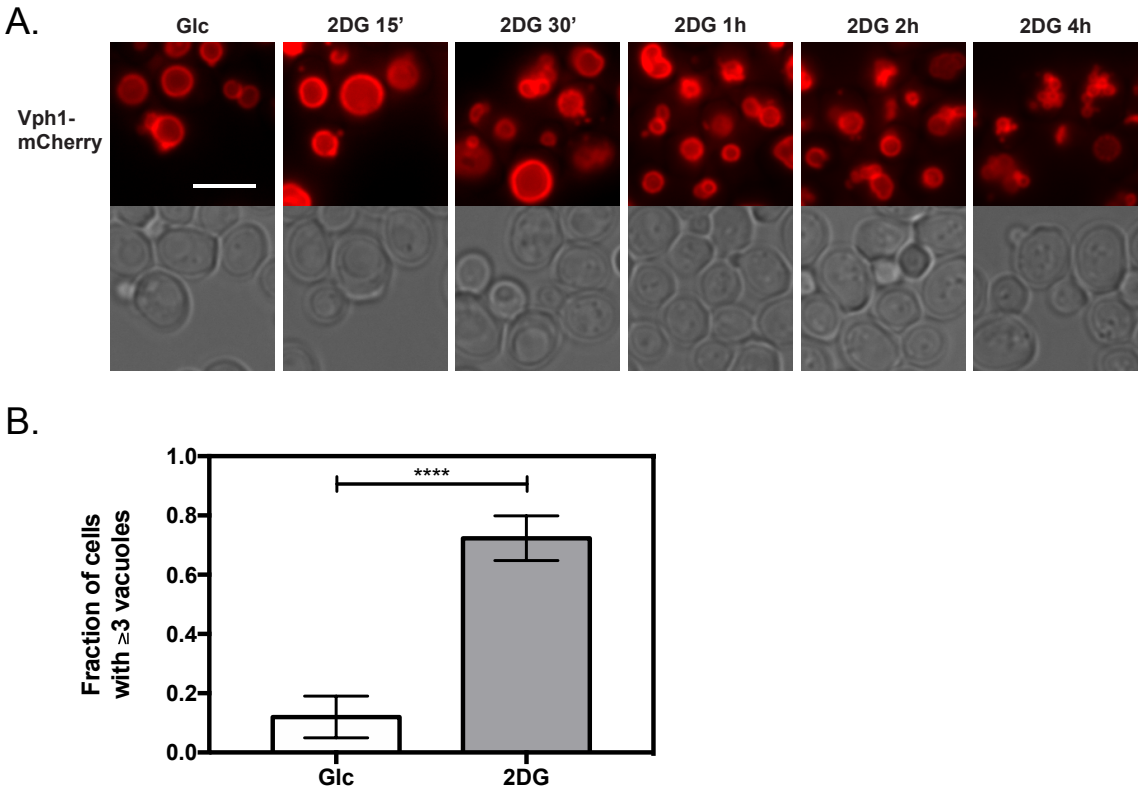

Laussel et al. Fig S1

Figure S1 - 2DG treatment induces vacuolar fragmentation. **A.** WT cells expressing Vph1 tagged with mCherry were grown overnight in glucose medium (exponential phase) and treated with 0,2% 2DG. Cells were collected and observed by fluorescence microscopy at the indicated times. Scale bar: 5 µm. **B.** Quantification of 2DG-induced vacuolar fragmentation (values ± SD, *n*=3 independent experiments, paired t-test).

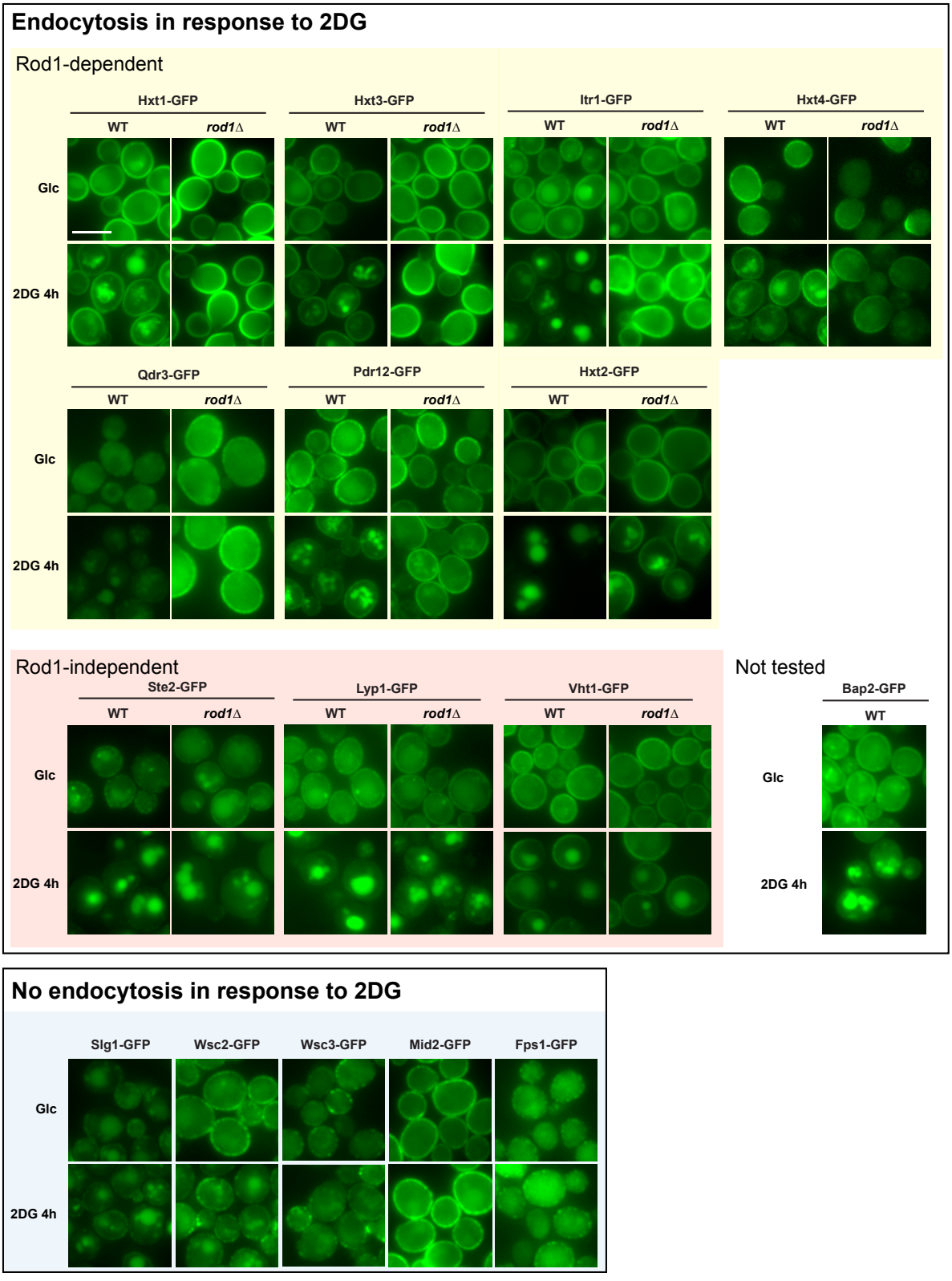

Laussel et al. Figure S2

989

Figure S2 - Most of the studied plasma membrane proteins are endocytosed in response to 2DG and this endocytosis is often Rod1-dependent. WT or *rod1Δ* cells expressing the indicated membrane proteins tagged with GFP at their endogenous genomic locus were observed by fluorescence microscopy before and after treatment with 2DG for 4h. Scale bar, 5 µm.

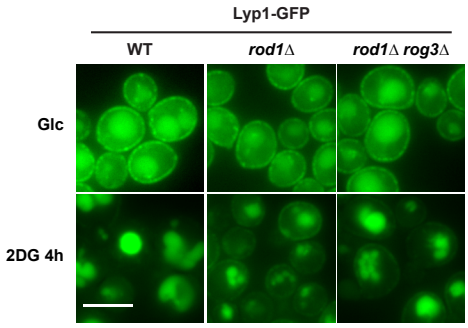

Laussel et al. Figure S3

994
995
996 **Figure S3 - Rog3 is not responsible for the observed Rod1-independent endocytosis of Lyp1-GFP in**
997 **response to 2DG.** WT, *rod1Δ* and *rod1Δ rog3Δ* cells expressing Lyp1-GFP tagged at its endogenous genomic
998 locus were observed by fluorescence microscopy before and after treatment with 2DG for 4h. Scale bar, 5 µm.
999

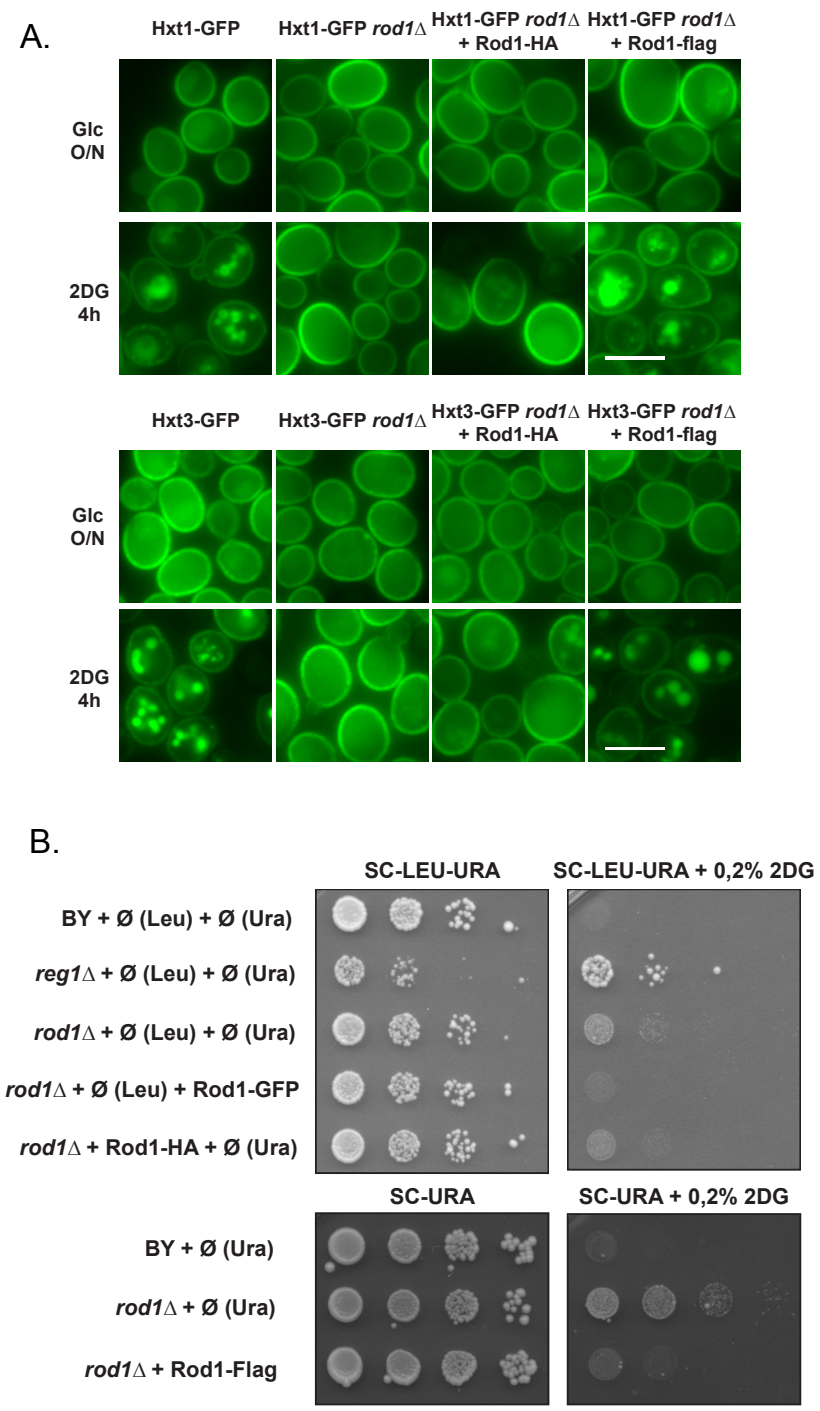

Laussel et al. Figure S4

Figure S4- Expression of Rod1-3HA does not restore endocytosis nor sensitivity to 2DG in a *rod1Δ* context, contrary to Rod1-Flag. (**A**) The indicated strains were observed by fluorescence microscopy after growth in a glucose-containing medium and after 2DG treatment for 4h. Scale bar, 5 µm. (**B**) Serial dilutions of cultures of the indicated mutants were spotted on dropout SC medium (SC) or SC + 0,2% 2DG and grown for 3 days at 30°C.

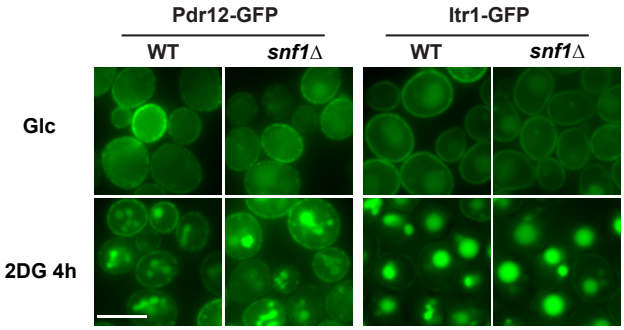

Laussel et al. Figure S5

Figure S5 - *SNF1* deletion is not sufficient to block endocytosis in response to 2DG. Pdr12-GFP, Pdr12-GFP *snf1Δ*, Itr1-GFP and Itr1-GFP *snf1Δ* cells were grown in a glucose-containing medium and observed by fluorescence microscopy before and after 2DG treatment for 4h. Scale bar, 5 µm